frontiers | Frontiers in Earth Science

TYPE Original Research
PUBLISHED 12 January 2023
DOI 10.3389/feart.2022.1089700

OPEN ACCESS

EDITED BY
Jiyuan Yin,
Chinese Academy of Geological Sciences (CAGS), China

REVIEWED BY
Xijun Liu,
Guilin University of Technology, China
Yongjiang Liu,
Ocean University of China, China

*CORRESPONDENCE
Qigui Mao,
qg-mao@ms.xjb.ac.cn
Wenjiao Xiao,
wj–xiao@mail.iggcas.ac.cn
Miao Sang,
sangmiao@ms.xjb.ac.cn

SPECIALTY SECTION
This article was submitted to Petrology, a section of the journal Frontiers in Earth Science

RECEIVED 04 November 2022
ACCEPTED 16 November 2022
PUBLISHED 12 January 2023

CITATION
Mao Q, Xiao W, Sang M, Ao S, Song D, Tan Z, Wang H and Li R (2023), Two different types of provenances and the amalgamation of subduction complexes in the Eastern Tianshan of the Southern Altaids.
Front. Earth Sci. 10:1089700.
doi: 10.3389/feart.2022.1089700

Two different types of provenances and the amalgamation of subduction complexes in the Eastern Tianshan of the Southern Altaids

Qigui Mao[1,2,3]*, Wenjiao Xiao[1,2,4,5]*, Miao Sang[1,2]*, Songjian Ao[4,5,6], Dongfang Song[4,5,6], Zhou Tan[1,2], Hao Wang[1,2] and Rui Li[1,2]

[1]State Key Laboratory of Desert and Oasis Ecology, Xinjiang Institute of Ecology and Geography, Chinese Academy of Sciences, Urumqi, China, [2]Xinjiang Research Center for Mineral Resources, Xinjiang Institute of Ecology and Geography, Chinese Academy of Sciences, Urumqi, China, [3]Redrock Mining Co. Ltd., Hami, China, [4]Innovation Academy for Earth Science, Chinese Academy of Sciences, Beijing, China, [5]College of Earth and Planetary Sciences, University of Chinese Academy of Sciences, Beijing, China, [6]State Key Laboratory of Lithospheric Evolution, Institute of Geology and Geophysics, Chinese Academy of Sciences, Beijing, China

The nature and final closure of the northern Tianshan Ocean have been debated in regard to the eastern Tianshan orogen, southern Altaids. The Kanguer subduction complex of the eastern Tianshan is the key to addressing these issues. In this study, we report new mapping, geochemical and geochronological results on the Kanguer subduction complex in the Haluo area. Our new results show that upper Permian (257 Ma) basaltic blocks emplaced in a sandstone matrix in the northern HL area are fragments of normal-mid-ocean-ridge-basalt (N-MORB)-type oceanic crust. The geochronological results indicate that the sandstone matrices display two different types of provenances. The first type in the northern part of the cross-section (till Sample YY12) has maximum depositional ages ranging from 316 Ma to 238 Ma. Their depositional settings varied from intraoceanic island arcs to continental Andean arcs after ca. 244 Ma, their detrital zircon age patterns vary from a single peak to multiple peaks, and their zircon $\varepsilon_{Hf}(t)$ values vary from uniquely high positive to some negative values. The second type is in the southern part of the cross-section with Samples YY12 to 21Kg05, which have the geochemical signatures of continental island arc sandstone, multiple-peak detrital zircon-age patterns, and positive to negative zircon $\varepsilon_{Hf}(t)$ values. The youngest sandstone sample has a maximum depositional age of 241 Ma. The above provenance results indicate that all mélanges and coherent units north of Sample YY12 belong to an accretionary complex of the Dananhu intraoceanic arc, and those south of Sample YY12 belong to an accretionary complex of the Yamansu-central Tianshan arc. According to the youngest components in both accretionary complexes, which suggest the latest subduction events, we conclude that the final amalgamation timing was after 238 Ma and that the Paleo-Asian Ocean closed during the Middle to Late Triassic.

KEYWORDS
detrital zircon, U-Pb ages, mélange, suture zone, Altaids

1 Introduction

The ophiolitic mélange in an accretionary complex is a set of tectonic complexes that are formed by long-term, complicated subduction and are scraped and stacked in the subduction zone. In general, the mélange consists of fragments of oceanic crust, oceanic islands, oceanic mountains, flysch, and different types of sedimentary rocks (Hsü, 1968; Isozaki et al., 1990; Zhang et al., 2012; Kusky et al., 2013; Xiao et al., 2015). The ophiolitic mélange is a significant unit of orogens and sedimentary records and can provide important information on the evolutionary processes of paleo-oceans and the tectonic patterns of paleo-plates. However, the amalgamation processes of different blocks are complicated, and the suture line and the final collisional time are usually difficult to constrain (Isozaki et al., 1990; Wakabayashi, 2015; Wakita, 2015).

The Altaids or the southern Central Asian Orogenic Belt, which is one of the largest accretionary orogens in the world (Figure 1A), accreted around and southward from the Siberian craton with many arcs, accretionary complexes and microcontinents in the Paleo-Asian Ocean (PAO, Bazhenov et al., 2003; Buchan et al., 2002; Coleman, 1989; Dobretsov et al., 1995; Şengör and Natal'in, 1996; Şengör et al., 1993; Wilhem et al., 2012; Windley et al., 2007; Xiao et al., 2018). The PAO had a paleogeography similar to that of the present SW Pacific, with multiple oceans, islands and subduction zones (Windley et al., 2007; Xiao et al., 2010). The Kanguer subduction complex (KGSC) occurs between the Dananhu intraoceanic arc and the Yamansu-central Tianshan (CTS) continental arc in the eastern Tianshan. It represents the subduction zone of the northern Tianshan Ocean which is a southern branch of the Paleo-Asian Ocean remnants (Xiao et al., 2004; Li et al., 2005; Chen et al., 2019; Ao et al., 2021). Therefore, the provenances of the sedimentary matrix in the accretionary complex of the Dananhu and Yamansu-CTS arcs may be significantly different (Maynard et al., 1982; Floyd and Leveridge, 1987; Floyd et al., 1991; Mader and Neubauer, 2004; Yan et al., 2016). Therefore, in regard to this critical accretionary complex, this study determines the constraints on the subduction tectonic processes of this ancient ocean and on the accretionary history and final amalgamation of the southern Altaids.

Several models have been proposed for the tectonics of the KGSC; however, the composition and tectonic nature of the subduction complex and the subduction polarity of the paleo-ocean are controversial and can be summarized as 1) the accretionary complex of the Dananhu (Li, 2004; Xiao et al., 2004; Li et al., 2005; Ao et al., 2021), 2) the accretionary complex of the Yamansu arc (Chen et al., 2019), and 3) the mixing of the forearc mélange between the Dananhu and Yamansu arcs (Muhetaer et al., 2010). The proposals for the time of final accretion and amalgamation vary from the Devonian (Xia et al., 2004; Wang et al., 2006) to the Carboniferous (Gao and Klemd, 2003; Zhou et al., 2004; Qin et al., 2011; Han and Zhao, 2018) to the latest Carboniferous-early Permian (Xiao et al., 2004; Zhang et al., 2018; Du et al., 2020) to the Middle-Late Triassic (Chen et al., 2020; Ao et al., 2021; Mao et al., 2022a; Mao et al., 2022b).

In this paper, we report our new lithological and structural mapping results of the KGSC in the Haluo (HL) area in eastern Tianshan (NW China), new geochronological and isotopic data of the sandstone matrix, and new geochemical data of basaltic blocks in the mélange, aiming to constrain the tectonics of the northern Tianshan Ocean and the final amalgamation processes of the southern Altaids.

2 Geological background

The eastern Tianshan occupies the southernmost Altaids (Figure 1A) and comprises E/W-trending continental margin arcs, microcontinents, island arcs, ophiolites, and accretionary wedges (Xiao et al., 2004; Li et al., 2006). The internal tectonic units of the orogen are as follows from north to south (Figure 1B): the Dannanhu arc, the Kanguer subduction complex, the Yamansu arc, the Central Tianshan (CTS) block, and the southern Tianshan accretionary complex. These tectonic units were accreted and amalgamated from Ordovician to Triassic and docked together during the closure of the Paleo-Asian Ocean in the Permian to the Triassic (Ma et al., 1997; Xiao et al., 2004; Li et al., 2006; Zhang et al., 2018).

The Dannanhu arc, which is an intraoceanic arc, is mainly composed of Ordovician to Permian tholeiitic basalts, calc-alkaline andesites, pyroclastic rocks, sedimentary rocks and granitoids (Xiao et al., 2004; Wang et al., 2018; Zhang et al., 2018; Mao Q. G. et al., 2021; Du et al., 2021). These magmatic rocks have subduction-related geochemical features with positive whole-rock $\varepsilon_{Nd}(t)$ (+0.6– +10.2) (Qin et al., 2011; Mao et al., 2014b; Du et al., 2018a; Wang et al., 2018; Zhang et al., 2018; Mao et al., 2019; Mao Q. G. et al., 2021) and zircon $\varepsilon_{Hf}(t)$ (+0.3– +19.6) values. The Yamansu arc consists of Devonian-Permian tholeiitic to calc-alkaline volcanic and intrusive rocks interbedded with sedimentary rocks with relatively low whole-rock $\varepsilon_{Nd}(t)$ (ca. −1.1– +7.1) and zircon $\varepsilon_{Hf}(t)$ values (ca. −3.4– +17.0) (Luo et al., 2016; Du et al., 2019; Long et al., 2020), which were interpreted as a continental arc built on the northern margin of the CTS Arc during the Devonian-Permian (Hou et al., 2014; Du et al., 2018b; Chen et al., 2019; Han et al., 2019; Zhao et al., 2019). The CTS comprises Paleozoic calc-alkaline basaltic andesites, volcaniclastic rocks, minor I-type granites, and

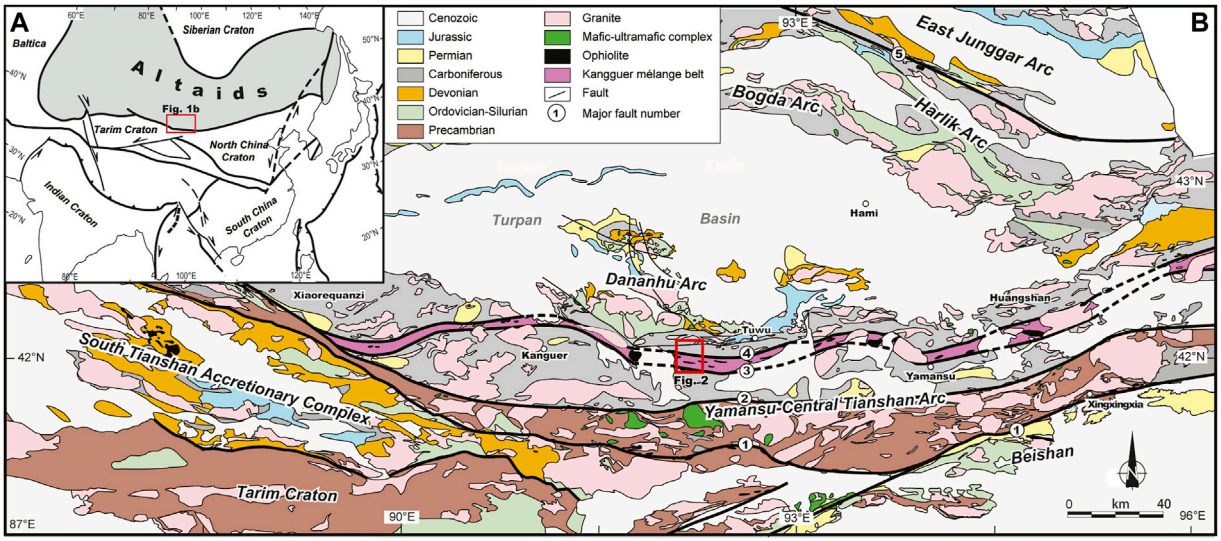

FIGURE 1
(A) Schematic tectonic map of Central Asia (Şengör et al., 1993; Xiao et al., 2018) showing the position of the eastern Tianshan in Figure 1B. **(B)** Geological map of the eastern Tianshan showing the distribution of the main tectonic units (modified after Xiao et al. (2004)). The locations of Figure 2 are marked. ① Kawabulake-Xingxingxia fault, ② Aqikekuduke-Shaquanzi fault, ③ Yamansu-Kushui fault, ④ Kanguer fault, and ⑤ Kalameili fault.

a Precambrian basement (Hu et al., 2000; Liu et al., 2004; Li et al., 2009; Mao et al., 2014a; Ma et al., 2014; Luo et al., 2016). The arc-related volcanic rocks and granitoids with relatively low whole-rock $\varepsilon_{Nd}(t)$ (ca. −5.7– +2.2) (Li et al., 2016; Lu et al., 2017; Mao et al., 2022a) and zircon $\varepsilon_{Hf}(t)$ values (ca. −15.4– +17.0) (Figure 8).

The Southern Tianshan accretionary complex contains discontinuous slices of Middle Devonian to early Carboniferous ophiolites (Gao and Klemd, 2003; Ao et al., 2020; Sang et al., 2020). The KGSC is located between the Dananhu arc in the north and the Yamansu-CTS arc in the south (Figure 1C). It was formed by long-lived northward subduction of the north Tianshan Ocean (a branch of the Paleo-Asian Ocean) and is composed of thrust-imbricated and dismembered serpentinite, ultramafic rocks, gabbro, basalt, limestone, and chert in a meta/deformed sandstone matrix. The gabbro and basalt blocks contain supra subduction zone (SSZ), normal-mid-ocean-ridge-basalt (N-MORB) and enriched mid-ocean ridge basalts (E-MORB) type ophiolite fragments (Xiao et al., 2004; Li et al., 2005; Li et al., 2006; Li et al., 2008; Chen et al., 2019; Ao et al., 2021).

3 Field geology of the Haluo area and sampling

The mélange in the Haluo (HL) area, which is located in the middle section of the KGSC, has a block-in-matrix structure with strong, nearly E–W-trending vertical cleavages. The blocks of sandstone and basalt belong to top-to-the-south thrust duplexes. The thrusts and cleavages of the KGSC in the entire HL area were displaced by late NW/SE-trending dextral strike-slip faults (Figure 2). At the map scale, the blocks of gabbro, massive basalt, diabase dikes, chert, limestone, and sandstone/siltstone are embedded and imbricated in a matrix of chlorite-phyllite schist and cleaved sandstone (Figures 2, 3A), and at the field scale, the oceanic and sedimentary rocks form a mutual matrix, e.g., the sedimentary rocks are the matrix, as shown in Figure 3A, and the strongly deformed basalts are the matrix as well (Figure 3B). The gabbro, basalt and chert blocks are highly cleaved (Figure 3C) and crop out in discontinuous lenses or ribbons ranging in length from several centimeters to several hundred meters (Figures 2A, 3C,D). The blocks of gabbro and basalt are elongated with their long axes aligned subparallel to the nearly E–W-trending faults in the mélange. The cherts generally crop out as lenses ranging in length from several meters to a kilometer with aspect ratios from 1:1 to 1:10 with their long axes parallel to the adjacent cleavage. The limestones crop out as discontinuous structural lenses or ribbon beds in the continuous sedimentary units. The matrix sandstones and chlorite-phyllite blocks display tectonic lenses and continuous bedding units and range in width from several meters to several kilometers and are tens of kilometers long. Most of them are highly cleaved and were intruded by volumes of quartz veins, indicating the movement of hydrothermal fluids during shearing (Figure 2A). The E–W-trending, subvertical cleavages in the matrix are penetrative and

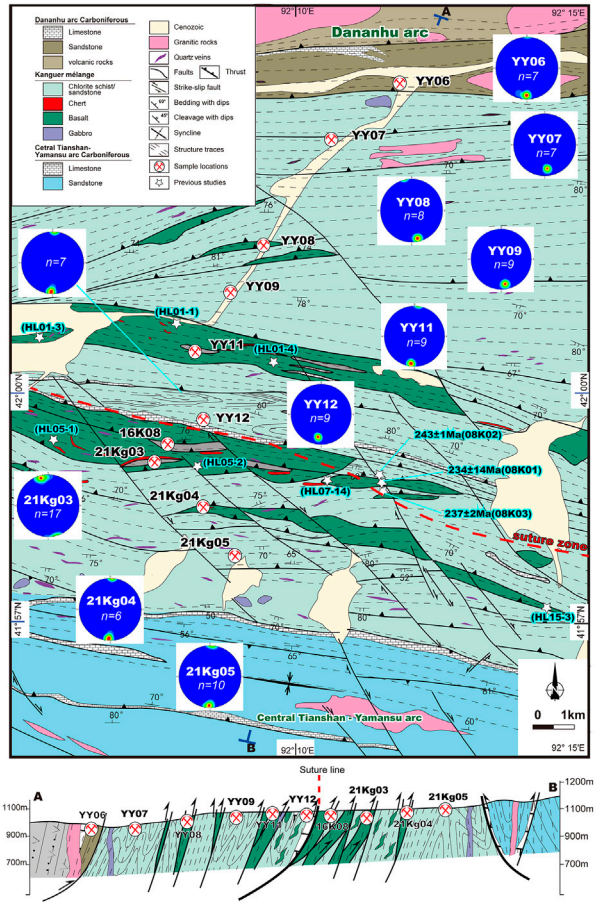

FIGURE 2
A geological map of the Kanguer subduction complex in the HL area showing the block-in-matrix structure. The sample locations and cross-section are marked. Stereographic projections of cleavages in the mélange matrix along the sections.

have overprinted the bedding so strongly that the primary depositional structures are mostly difficult to observe (Figure 2A). Some places have primary sedimentary bedding that can be distinguished, such as in the northern, central and southern continuous units of the mélange.

The KGSC in the HL area was thrusted southward; most of the blown sandstones, white limestone, red cherts, and massive green basalt blocks were thrusted to the south (Figures 2, 3A,B), but in some places, they also display northward thrusting, as shown in Figures 3C,D. Both the basalt and chert blocks are more strongly cleaved close to their whole bordering thrust planes (Figures 2, 3A–C). Some folds can be distinguished in the continuous sandstone blocks in the northern, central and southern parts of the HL area. Folded bedding planes parallel to the NE-trending cleavage indicate tight to isoclinal subvertical folds in the sandstone (Figure 2). Some elongated granitoid and gabbro dikes/intrusions intrude the mélange in the northern and southernmost HL area and are weakly cleaved; the long axes of the granitoid intrusions are parallel to the regional cleavage. Overall, these structures indicate regional N–S compression. All these compositions and structures indicate that the blocks of basalt, diabase, gabbro, limestone, sandstones and chert probably formed in different environments and were intermixed during subduction processes.

Two basalt samples (YY08-3 and YY08-6) were collected at location YY08 to analyze the zircon U–Pb ages, Hf isotopes and whole-rock geochemistry. The basalt is highly chloritized and epidotized, and consists of plagioclase, pyroxene, magnetite, ilmenite, minor olivine and clinopyroxene phenocrysts (Figures 4A,B). Eight sandstone samples in the NS-trending cross-section were collected for detrital zircon U–Pb dating and Hf isotope analysis. Most of them have deformed (Figure 4). The coarse-grained sandstone comprises angular plagioclase, quartz and lithic fragments (e.g., Samples 16K08 and 21Kg05, Figures 4C,D). The sandstones are composed of directionally arranged quartz, plagioclase and minor lithic fragments (e.g., Samples YY07, YY09, and YY12, Figures 4E,F,G). The tuffaceous siltstone consists of quartz and tuff/clay (Samples YY11 and 21Kg04, Figures 4H,I).

4 Zircon U–Pb age and Hf isotopes

4.1 Basalt

Zircons from basalt Sample YY08 in the northern part of the Kanguer accretionary complex are 50–120 μm long and have length/width ratios of 1.0–1.5, with magmatic oscillatory zones in cathodoluminescence (CL) images (Figure 5B), and they have variable Th/U values of 0.33–0.91. Fifteen zircon grains were analyzed, and fourteen of them yielded concordant ages with $^{206}Pb/^{238}U$ ages scattered from 361 Ma to 254 Ma (Figure 5A). There are three groups of grains that have mean weight ages of 257 ± 15 Ma (MSWD = 10, n = 3), 296.6 ± 6.4 Ma (MSWD = 6.6, n = 9) and 359.4 ± 6.0 Ma (MSWD = 0.29, n = 2). The older zircon grains were the precursor or xenocrysts of early magmatic events with $\varepsilon_{Hf}(t)$ values of +6.2 to +15.2, while the youngest three grains were the products of crystallization of the magma with high positive $\varepsilon_{Hf}(t)$ values of +7.3 to +11.1.

4.2 Sedimentary matrix sandstone

A total of 771 analyzed grains from nine sandstone matrix samples were collected along the NS-trending cross-section of the KGSC in the HL area (Figure 2). Seven hundred and ten analyzed grains yielded concordant ages (concordance % > 90% or <110%). All U–Pb and Lu–Hf isotopic data are shown in Supplementary Tables S1, S2, respectively. Only concordant ages are described and discussed below from north to south.

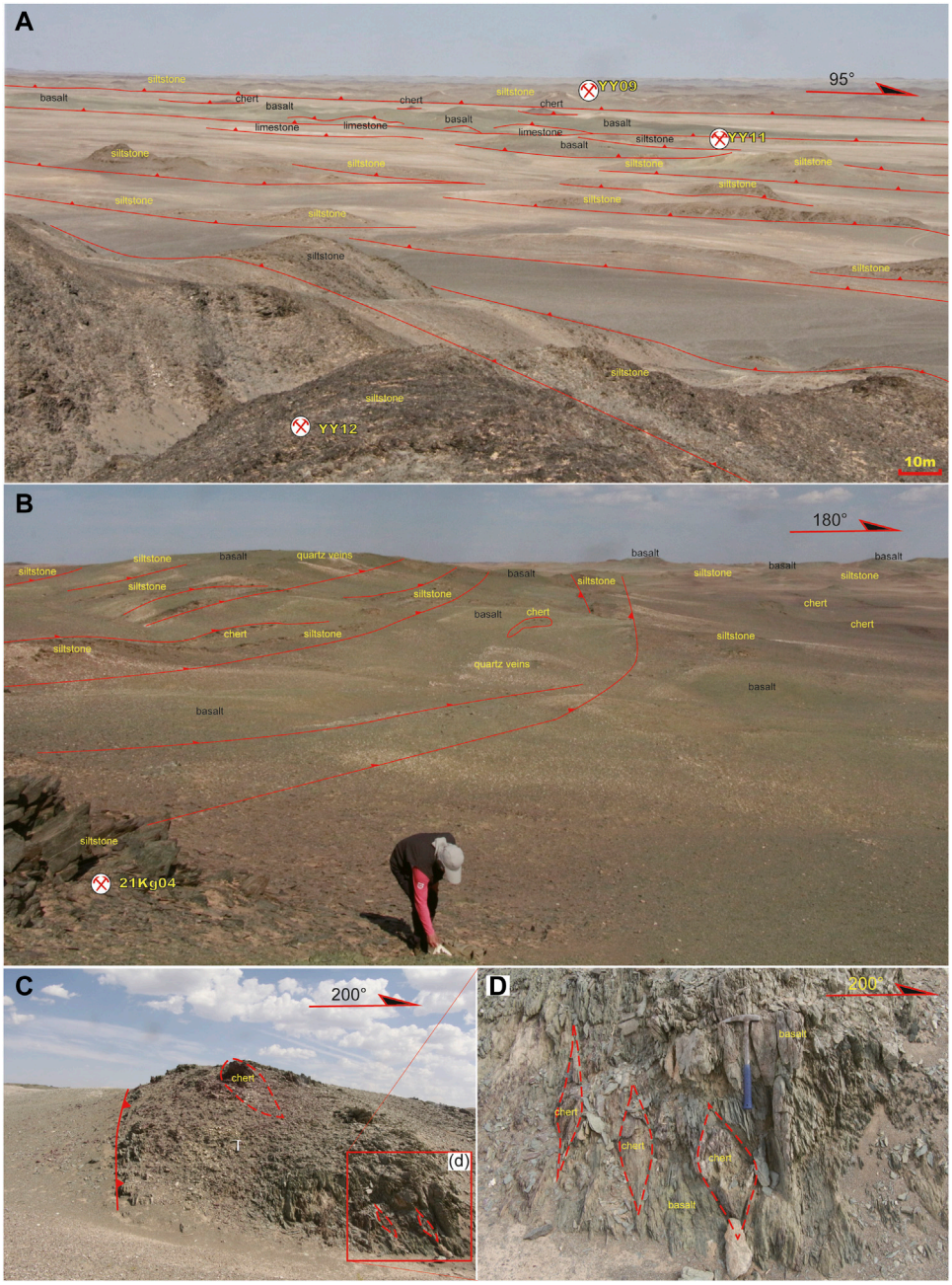

FIGURE 3
(A) Field photograph of the northern part of the HL area showing the block-in-matrix structure. **(B)** Field photograph of the southern part of the HL area showing the sedimentary blocks in the basalt matrix. **(C)** and **(D)** Photographs of strongly deformed basalt–chert blocks in the cleaved sedimentary rocks.

Several methods can calculate the maximum depositional age (MDA) of sedimentary rocks from their detrital zircon U–Pb ages, e.g., the youngest grain, the youngest three grains and the youngest peak (Coutts et al., 2019). Here, we use the weighted average ages of the youngest three grains if they overlap with a 2σ uncertainty or the youngest grain if the ages of the youngest three zircons far exceed a 2σ uncertainty [or the mean squared weighted deviation (MWSD) is poor].

4.2.1 Sample YY07

The zircons have grain sizes of 80–120 μm with length/width ratios of 1.2–1.8 and clear oscillatory zones in CL images. The

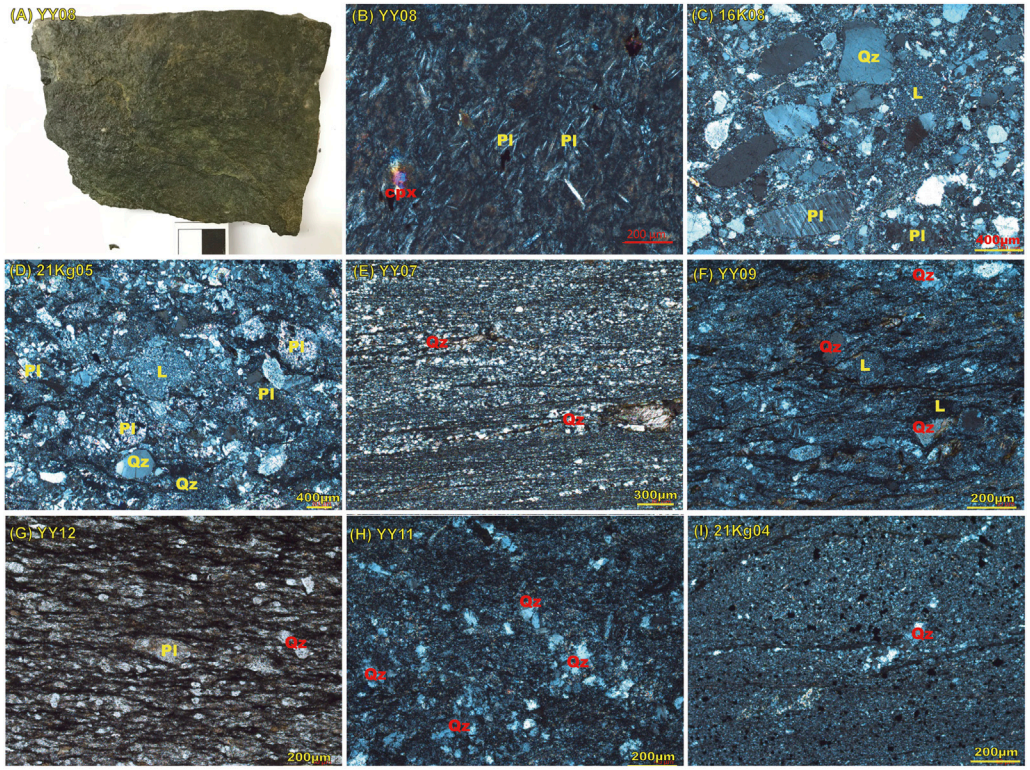

FIGURE 4
Photographs and Microphotographs of dated the samples. **(A)** Photographs of the basaltic sample YY08, **(B)** Microphotographs of the basaltic sample YY08, showing it comprises the clinopyroxene phenocrysts and plagioclase. **(C,D)** Microphotographs of coarse-grained sandstones (16K08 and 21Kg05), showing directionally, poor sorting and high proportions of detrital altered matrix. Grains are angular and subrounded. **(E–G)** Microphotographs of sandstones, showing directionally and poor sorting, high proportions of detrital and diagenetically altered matrix and a mix of quartz, feldspar and lithic framework fine grains. **(H,I)** Microphotographs of tuffaceous siltstones (YY11 and 21Kg04) consists of quartz and tuff/clay.

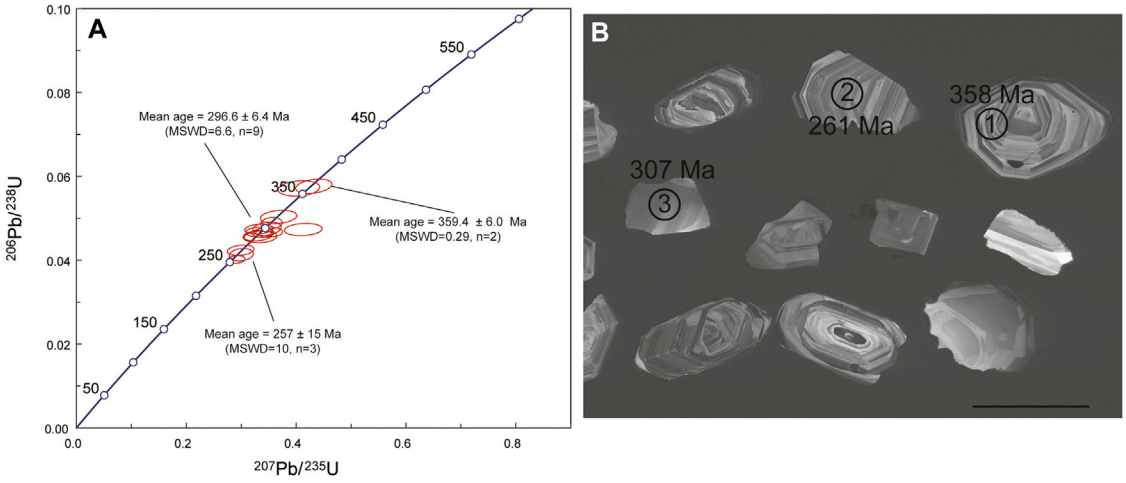

FIGURE 5
Concordia U–Pb diagrams **(A)** and CL images **(B)** for the zircons of the basalt fromf the north HL area.

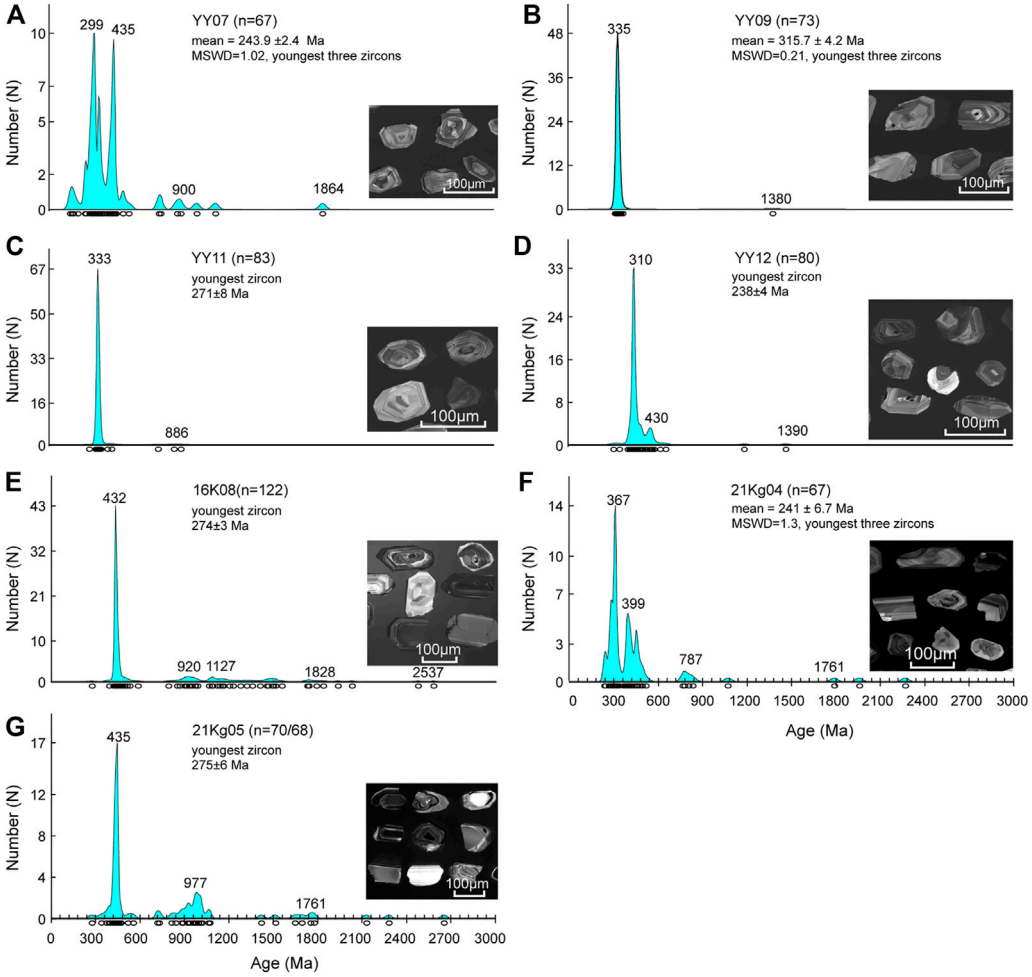

FIGURE 6
Histograms for the detrital zircons of the sandstones in the HL area (see Figure 2 for sample locations and supporting information and Supplementary Table S3 for data sources). **(A)** Sample YY07 of the north HL area shows multiple peaks detrital zircon age pattern. **(B), (C)**, and **(D)** Samples YY09, YY11 and YY12 of the north HL area show single peaks detrital zircon age patterns. **(E), (F)**, and **(G)** Samples 16K08, 21Kg04 and 21Kg05 of the south HL area show multiple peaks detrital zircon age patterns. Ages of 206Pb/238U and 1σ, with concordance % > 90% or < 110%, were used for density plots using DensityPlotter software Version 8.5 (Vermeesch, 2012).

concordant zircons have variable Th/U values of 0.25–2.04. Sixty-seven of the ninety-three analyzed grains yielded concordant ages ranging from 244–1,861 Ma. They have two main peaks at 299 and 435 Ma and three subordinate peaks at 240, 900, and 1,864 Ma (Figure 6A). The three younger ages yielded a weighted mean age of 243.9 ± 2.4 Ma (MSWD = 1.02). The $\varepsilon_{Hf}(t)$ values of the detrital zircons range from −18.0 to +15.6 (Figure 7C) and have 28% (18 grains in 65 analyzed grains) analyzed grains have negative $\varepsilon_{Hf}(t)$ values.

4.2.2 Sample YY09

The zircon grains are 100 μm long, and they have length/width ratios of 1–2.0 and prominent oscillatory zones in CL images (Figure 6B). Furthermore, they have variable contents of Th (56–910 ppm) and U (55–738 ppm) and Th/U values of 0.43–1.71. Of the ninety analyzed zircon grains, seventy-three grains yielded concordant ages with major concordant age peaks at 335 Ma (99% of the total), and only one grain has a Precambrian age of 1,380 ± 31 Ma (Figure 6B). The youngest three zircons yielded a weighted mean age of 315.7 ± 4.2 Ma (MSWD = 0.21). Lu–Hf isotope analyses of the concordant zircons yielded $\varepsilon_{Hf}(t)$ values ranging from +4.1 to +16.7 (Figure 7B).

4.2.3 Sample YY11

The zircons are 50–120 μm long and have length/width ratios of 1.0–2.0, with oscillatory zones in CL images. They have variable Th/U values of 0.22–1.37. Of the ninety analyzed zircon grains, eighty-three grains yielded concordant ages with major concordant age peaks at 333 Ma (91.6% of the total), and

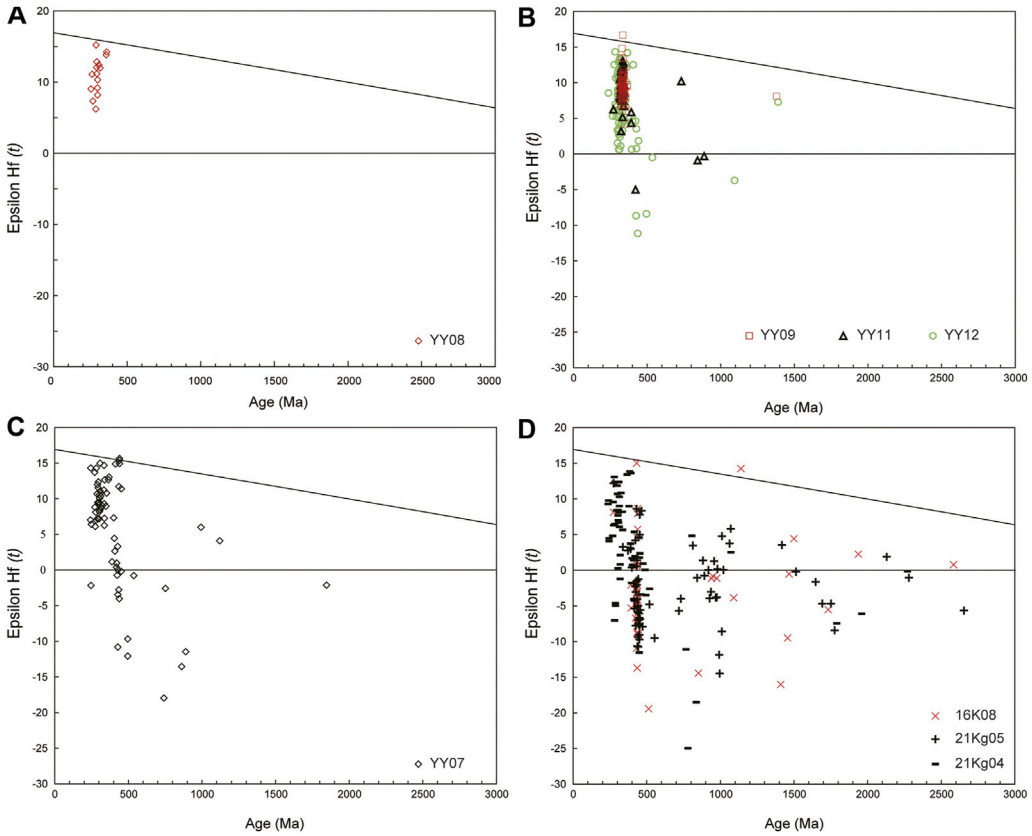

FIGURE 7
Hf isotope diagrams of dated samples. **(A)** Basalt from the northern HL area. **(B)** Samples YY09 and YY11 in the northern HL area showing that the sandstone samples were probably derived from the Dananhu intraoceanic arc to the north. **(C)** Samples YY07 and YY12 in the northern HL area show a small amount of material sourced from the Yamansu-central Tianshan arc to the south. **(D)** Samples 16K08, 21Kg04 and 21Kg05 in the southern HL area showing that the sandstones were probably derived from the Yamansu-central Tianshan arc to the south. The age data after Supplementary Table S3.

only three grains yielded Precambrian ages at 886, 843, and 733 Ma. The youngest zircon has an age of 271 ± 8 Ma, which is interpreted as the MDA of the sandstone (Figure 6C). Lu–Hf isotope analyses of the detrital zircons yielded $\varepsilon_{Hf}(t)$ values ranging from −5.1 to +13.1 (Figure 7B) and only three grains in 83 ananlyzed grains (ca. 4%) have negative $\varepsilon_{Hf}(t)$ values.

4.2.4 Sample YY12

Ninety zircon grains were analyzed, and seventy-nine grains yielded concordant ages with variable Th/U values of 0.08–1.06. Most of them have oscillatory zones in CL images. They have a major concordant age peak at 310 Ma and a second age peak at 430 Ma; only two grains yielded Precambrian ages at 1,095 and 1,390 Ma (Figure 6D). The youngest zircon has an age of 238 ± 4 Ma, which is interpreted as the MDA of the sandstone. Lu–Hf isotope analyses of the detrital zircons yielded $\varepsilon_{Hf}(t)$ values ranging from −11.2 to +14.3 (Figure 7C) and only six grains in 79 analyzed grains (ca. 8%) have negative $\varepsilon_{Hf}(t)$ values.

4.2.5 Sample 16K08

One hundred and twenty-nine zircon grains from Sample 16K08 were analyzed. One hundred and twenty-four zircon grains yielded concordant ages with variable Th/U values of 0.01–2.23. Most of them have oscillatory zones in CL images. These detrital zircons have multiple concordant age major peaks at 432 Ma and small peaks at 920, 1,127, 1,828, and 2,500 Ma (Figure 6E). The youngest zircon yielded a concordant age of 274 ± 3 Ma, which we interpret as the MDA of the sandstone. The detrital zircons have relatively variable $\varepsilon_{Hf}(t)$ values ranging from −19.4 to +15.0 (Figure 7D) and ca. 78% of 58 analyzed grains have negative the $\varepsilon_{Hf}(t)$ values.

4.2.6 Sample 21Kg04

All seventy analyzed zircon grains yielded concordant ages with variable Th/U values of 0.07–2.02. Most of them have oscillatory zones in CL images. The zircons display three major concordant age peaks at 367, 399, and 787 Ma, and

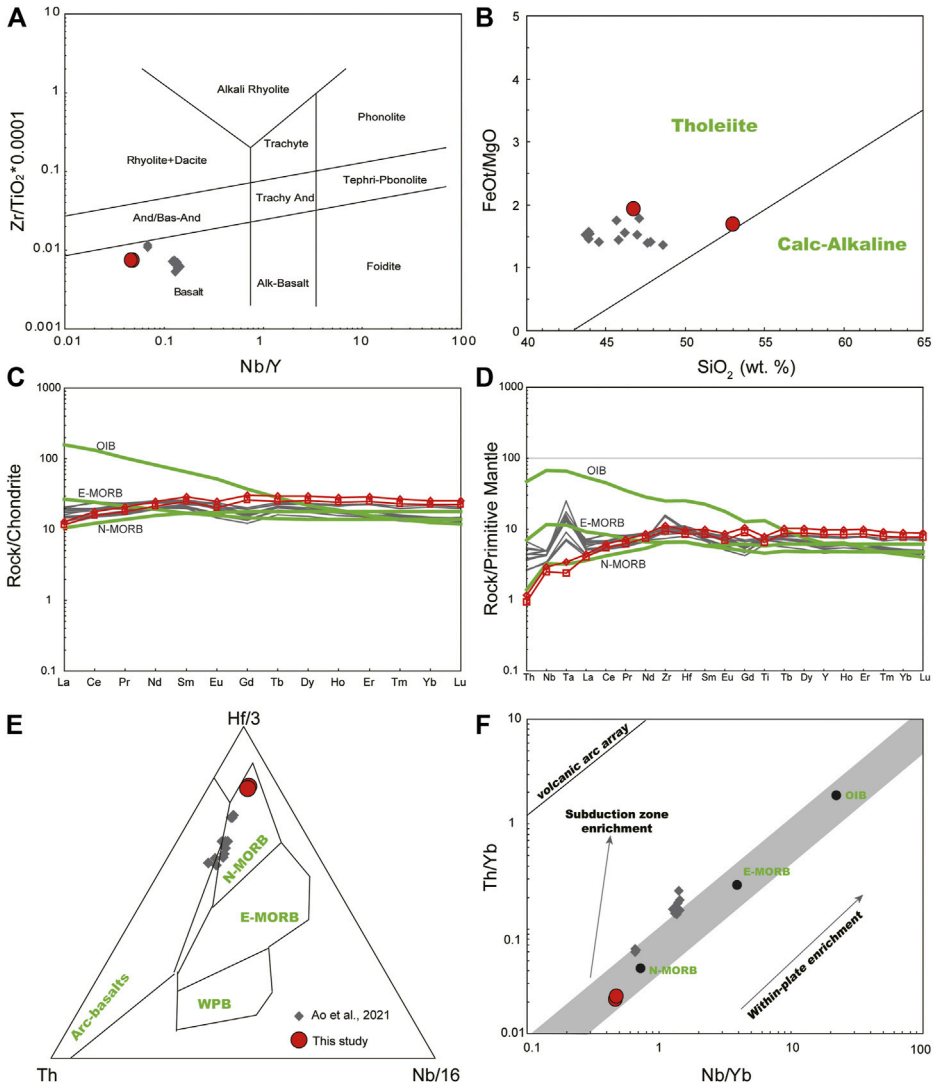

FIGURE 8
Geochemical diagrams of the basalt in the northern HL area of the KGSC. **(A)** Zr/Ti vs. Nb/Y diagram (Winchester & Floyd, 1977) and **(B)** FeO_t/MgO vs. SiO_2 diagram (Myashiro, 1974), **(C)** Chondrite-normalized REE and **(D)** primitive mantle normalized multielement diagrams. Chondrite values are from a previous study (Boynton, 1984). The PM values are from a previous study (Sun and McDonough, 1989). **(E)** Hf-Th-Ta diagram (Hawkins, 2003; Wood, 1980) and **(F)** Nb/Yb vs. Th/Yb diagram (Pearce, 2008). The fields of the Tofua Arc, Lau Basin and Mariana Trough are from Hawkins (2003). The basaltic fragments in the northern HL area are similar to those of N-MORBs. The dark diamonds and lines are after Ao et al. (2021).

the other four Precambrian zircon grains yielded ages of 1,073, 1,791, 1,960, and 2,302 Ma (Figure 6F). The youngest three zircon weight average ages are 241 ± 6.7 Ma (MSWD = 1.3), which we interpret as the MDA of the sandstone. The detrital zircons have relatively high $\varepsilon_{Hf}(t)$ values ranging from −35.6 to +13.9 (Figure 7D) and ca. 33% of 66 analyzed grains have negative the $\varepsilon_{Hf}(t)$ values.

4.2.7 Sample 21Kg05

The zircons have grain sizes of 80–120 μm with length/width ratios of 1.0–1.5 and clear oscillatory zones in CL images. Sixty-eight of the seventy analyzed zircon grains yielded concordant ages with variable Th/U values of 0.31–1.70. They have three major concordant age peaks at 435, 977, and 1,761 Ma, and three Paleoproterozoic to Neoarchean zircon grains yielded ages of 2,130, 2,281, and 2,655 Ma (Figure 6G). The youngest zircon has a concordant age of 275 ± 6 Ma, which is interpreted as the MDA of the sandstone. The detrital zircons have widely variable $\varepsilon_{Hf}(t)$ values ranging from −14.5 to +12.2 (Figure 7D) and ca. 66% of 68 analyzed grains have negative the $\varepsilon_{Hf}(t)$ values.

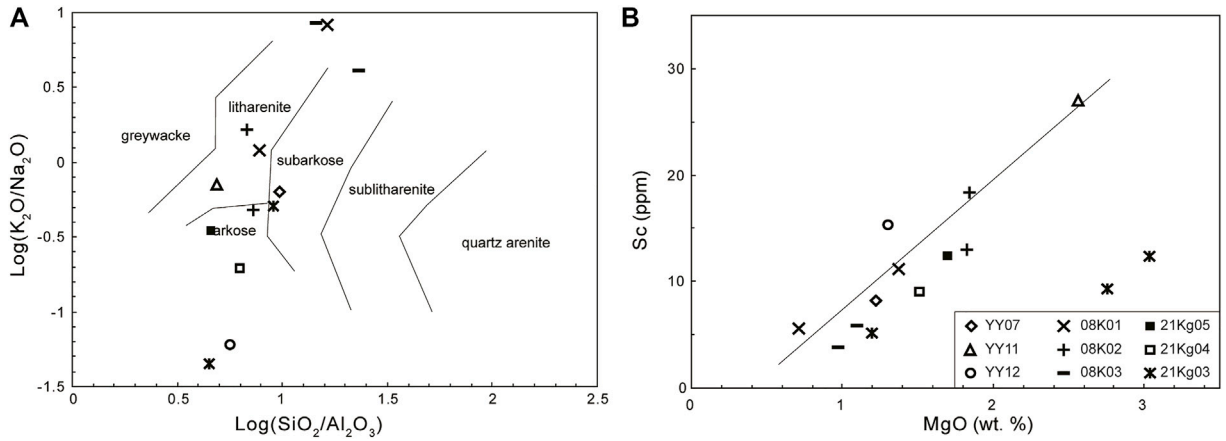

FIGURE 9
Chemical classification diagrams discriminating sedimentary rocks. **(A)** SiO_2/Al_2O_3 vs. Na_2O/K_2O (Pettijohn et al., 1972) and **(B)** MgO vs. Sc diagrams.

5 Geochemistry

5.1 Basalt

Two alternating basalt samples from the KGSC are the tholeiite basalts in the northern HL area (Figures 8A,B), which have moderate TiO_2 (1.4–1.7 wt.%) and relatively narrow elemental ratios with SiO_2 = 46.8–53.0 wt.%, Al_2O_3 = 12.3–13.3 wt.%, and CaO = 6.1–10.1 wt.%. They have high MgO (6.0–6.6 wt.%) contents and Mg# values of 52–55. The samples are altered and thus have variable loss on ignition (LOI) contents ranging from 4.8 to 5.9 wt.%. Their Na_2O concentrations vary from 0.78 to 3.71 wt.%, likely reflecting seawater alteration. They have right-obliquely depleted rare earth element (REE) patterns ($(La/Yb)_N$ = 0.4–0.53) that are similar to those of N-MORBs (Figure 8C) and slightly negative Eu anomalies (Eu* = 0.80–0.84). They also display right-oblique trace patterns ($(Nb/La)_{PM}$ = 0.67 $(Th/Nb)_{PM}$ = 0.40) and are slightly depleted in Ti on a primitive mantle-normalized spider diagram (Figure 8D).

5.2 Sedimentary matrix sandstone

The whole-rock geochemical data of these sandstones are listed in Supplementary Table S2. The SiO_2 contents (65.8–76.7 wt.%) and K_2O/Na_2O ratios (0.06–0.71) of sandstone in the northern HL area are lower than those in the southern HL area (74.1–88.7 wt.% and 0.48–8.39, respectively), but the Al_2O_3 contents of the sandstone in the northern HL area are higher (7.95–13.56 wt.%) than those in the southern HL area (3.82–10.88 wt.%). The SiO_2/Al_2O_3 ratios of the northern sandstones (4.86–9.46) are lower than those of the southern sandstones (6.81–23.24), indicating low clay and feldspar contents but high quartz contents in the protolith of the southern sandstone (Potter, 1978). On the SiO_2/Al_2O_3 vs. K_2O/Na_2O diagram (Figure 9A), the northern analyzed samples plot within the subarkose and litharenite fields, and the southern samples mainly plot as litharenite. All samples have a good positive Sc-MgO correlation (Figure 9B), indicating that abundant mafic clasts were contained within their protolith, which is supported by their petrological results.

The samples from the northern and southern HL areas have variable concentrations of REEs (64.9–141.1 ppm and 39.9–104.5 ppm, respectively) with similar chondrite-normalized REE patterns (Figures 10A,C). They are enriched in light rare earth elements (LREEs) with $(La/Yb)_N$ values of 3.18–5.95 and 4.82–11.0 and distinct Eu anomalies with Eu/Eu* values of 0.65–0.74 and 0.65–1.10, respectively. In comparison with the average upper continental crust (UCC), all samples show distinct negative Nb, Ta and Ba anomalies but higher enrichments in V, Cr, Ni, Sc, Cs, Ti and Y and negative to positive Sr (Figures 10B,D). This pattern is similar to that of the sandstones in the continental arc and active margin (Floyd et al., 1991).

6 Discussion

6.1 Nature of the northern Tianshan Ocean

Several competing models have been proposed for the northern Tianshan Ocean and can be summarized as follows: 1) an interarc basin between the Dannanhu and Yamansu arcs (Li, 2004; Xiao et al., 2004; Han and Zhao, 2018), 2) a short-lived limited ocean or back-arc basin in the Carboniferous (Ma et al., 1997; Wang et al., 2006; Wang et al., 2019), 3) a branch of the

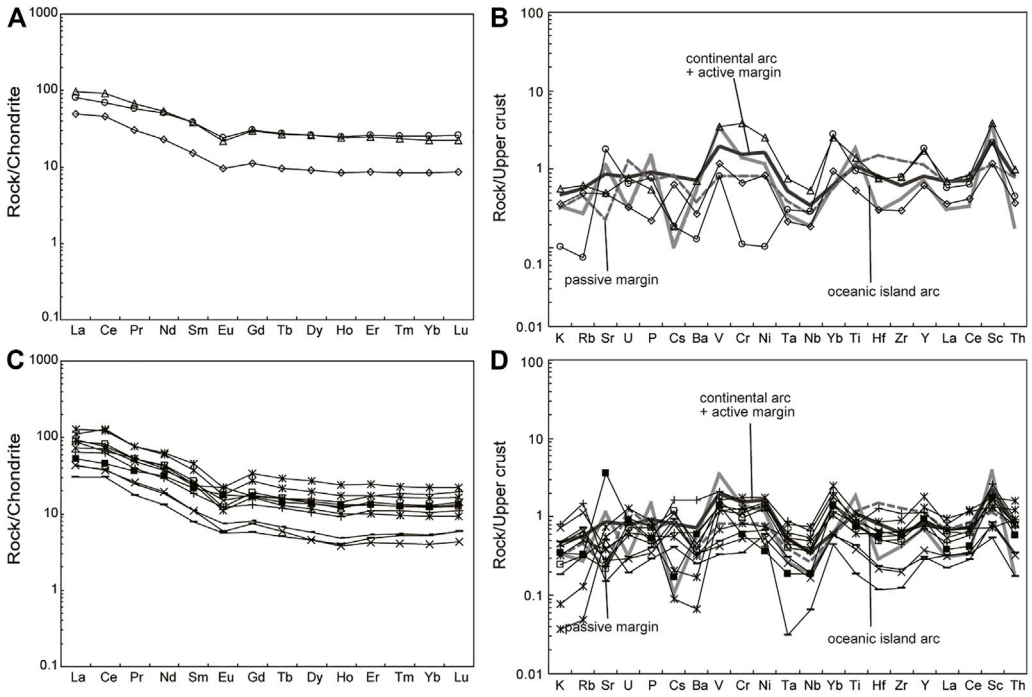

FIGURE 10
Chondrite-normalized REE diagram and multielement diagrams normalized to average upper continental crustal values (Floyd et al., 1991). **(A)** and **(B)** are the sandstone samples of the north KGSC in HL area, **(C)** and **(D)** are the sandstone samples of the south KGSC in HL area. The chondrite values are from a previous study (Boynton, 1984). The cited passive margin, oceanic island arc and continental arc island arc+ active continental margin values are from Floyd et al. (1991). The symbols used are the same as those used in Figure 9.

Paleo-Asian Ocean that separated the Siberian craton to the north and the Tarim craton to the south (Li et al., 2005; Li et al., 2008; Chen et al., 2019; Mao et al., 2019; Ao et al., 2021), and 4) a short-lived, limited-rifted ocean on the accretionary wedge in the Carboniferous to Permian (Wang et al., 2006; Wang et al., 2019).

Our zircon LA-ICP–MS U–Pb dating reveals that the basaltic rocks have crystallization ages of 257 Ma. In addition, Li et al. (2008) reported that the gabbro of the Kanguertage ophiolite yielded a zircon SHRIMP U–Pb age of 494 ± 10 Ma. Therefore, direct geochronological studies of oceanic crust fragments suggest that the northern Tianshan Ocean was a long-lived ocean with an age of >ca. 494 Ma to <ca. 257 Ma. The zircon U–Pb dating of the sedimentary matrix in the KGSC reveals MDAs ranging from 384 to 234 Ma (Chen et al., 2019; Ao et al., 2021) and arc-related magmatism ages from the Ordovician to Triassic in the Dananhu arc (ca. 453 Ma to 234 Ma) and Yamansu-CTS arc (ca. 481 Ma to 234 Ma) (Xiao et al., 2004; Zhang et al., 2018; Chen et al., 2019; Du et al., 2019; Long et al., 2020; Mao Q. et al., 2021; Mao Q. G. et al., 2021; Du et al., 2021; Mao et al., 2022a). All of these data suggest that the northern Tianshan Ocean was a long-lived ocean (494 Ma to ca. 234 Ma).

The KGSC in the map area is characterized by "block-in-matrix" structures and was thrust-imbricated (Ao et al., 2021, this study). The field relationships and structural characteristics indicate that the HL area is a classic ophiolitic-bearing tectonic mélange that formed at a convergent margin and was created by subduction–accretion processes (Wakabayashi, 2015; Xiao et al., 2015; Kusky et al., 2020; Ao et al., 2021). Basalt, diabase, gabbro, limestone, and chert represent fragments of oceanic crust that can provide information on the nature and history of the oceanic plate (Xiao et al., 2015; Festa et al., 2019; Raymond, 2019; Wakabayashi, 2019; Kusky et al., 2020). Our studies reveal that the basaltic fragments from the northern parts of the HL area are tholeiitic rocks and have typical N-MORB geochemical signatures with right-oblique depleted REE patterns ($(La/Yb)_N$ = 0.4–0.53) and trace patterns (Figures 8C,D) and high zircon Hf isotope values (+9.0–+14.4). They have relatively high Zr/Nb (59.0–59.7) and La/Nb (1.44–1.57) and higher Th/Nb (0.04–0.05) ratios, which are similar to those of N-type MORB basalts (>30, 1.07 and 0.05) (Sun and McDonough, 1989; Wilson, 2001). On Hf-Th-Nd and Th/Yb-Nb/Yb diagrams (Figures 8E,F), the basalts plot in the N-MORB field. Thus, all geochemical and Hf isotope features demonstrate that these basalts were probably generated in a mid-ocean ridge, where erupted lavas were influenced by seawater penetration. This conclusion is consistent with the ophiolitic fragments in the southern part of the map area, which have N-MORB to SSZ ophiolitic fragments (Figures 8E,F), suggesting that the northern Tianshan Ocean contained typical N-MORB oceanic crust (Ao

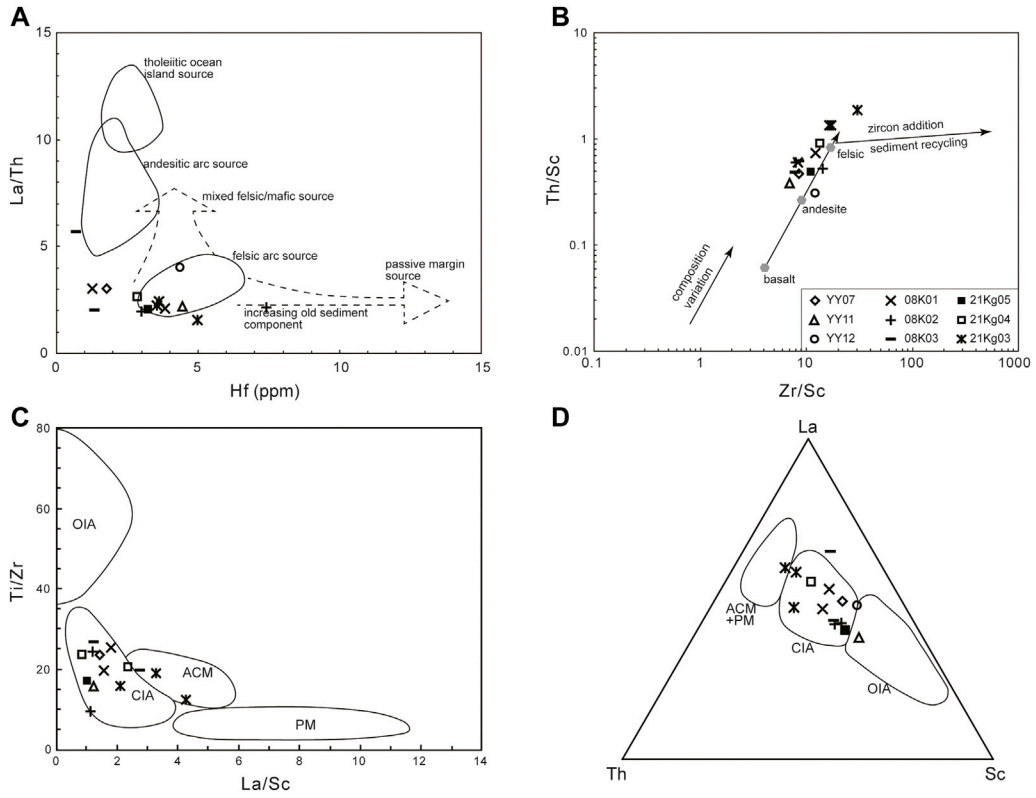

FIGURE 11
Tectonic setting discrimination diagrams for the sandstone matrix in the KGSC in the HL area. **(A)** Hf vs. La/Th diagram (Floyd and Leveridge, 1987), **(B)** Th/Sc vs. Zr/Sc diagram (McLennan et al., 1993), **(C)** La/Sc vs. Ti/Zr, **(B)** Th-Co-Zr/10 and **(D)** La–Th–Sc plots (Bhatia and Crook, 1986). ACM, active continental margin; PM, passive continental margin; CIA, continental island arc; and OIA, oceanic island arc.

et al., 2021). Previous studies have also suggested that the KGSC contains SSZ-, N-MORB- and E-MORB-type oceanic fragments, e.g., 1) some basalt fragments in the middle part of the map area have SSZ and N-MORB ophiolitic geochemical characteristics (Ao et al., 2021); 2) the E-MORB- and N-MORB-type ophiolitic blocks in the Yamansu area (Chen et al., 2019); and 3) the SSZ-type ophiolitic blocks in the Kanguertage area in the western section of the KGSC (Li et al., 2005; Li et al., 2008). These geochemical signatures of the ophiolitic fragments of the KGSC indicate that the northern Tianshan oceanic crust was as complicated as the Pacific oceanic crust.

In summary, the geological, geochemical and geochronological features of the ophiolitic fragments of the KGSC, together with data from the Dananhu arc and Yamansu-CTS arc, suggest that the northern Tianshan Ocean was a branch of the Paleo-Asian Ocean. The northern Tianshan Ocean born before 497 Ma, and N-MORB and E-MORB type ophiolites were formed by the normal middle oceanic-ridge and hotspot, respectively. The subduction formed the SSZ-type ophiolite and caused the different oceanic crust to be accreted in the Kanguer subduction complex during Cambrian to Triassic.

6.2 Two types of provenances for the sedimentary matrix in the Kanguer subduction complex

The matrix of the accretionary complex originates from arcs and/or forearcs sedimentary rocks. Therefore, the provenance variations in the matrix can provide detailed information on the spatiotemporal framework of the arcs, the subduction polarity and the evolution of the subduction. Therefore, the two arcs were the main potential provenance for the sandstone matrix of the KGSC.

Basalt and rhyolite detrital fragments in the sandstone indicate a mixed origin (Figure 4). The angular clastic and euhedral detrital zircon grains (Figures 4, 6) indicate that they had a proximal source and were deposited on an active margin (Floyd and Leveridge, 1987). The significant enrichment of LREEs and the flat HREE patterns (Figures 10A,C) also imply a felsic source, which is also attested by a plot of La/Th against Hf (Figure 11A). On the Th/Sc vs. Zr/Sc diagrams (McLennan et al., 1993), the samples plot along the compositional variation line from the area of felsic volcanic rocks to the

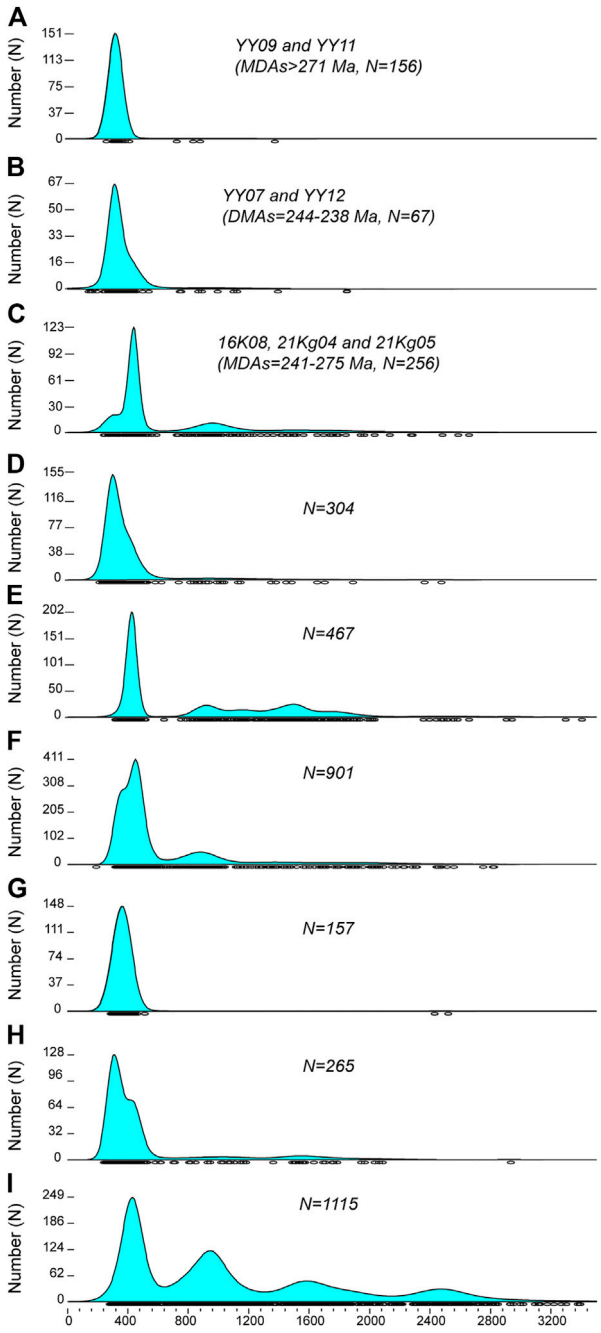

FIGURE 12
Comparison of probability plots for zircon U–Pb ages of sedimentary rocks around the KGSC. **(A)** The sandstone matrix (MDAs > ca. 244 Ma, Samples YY09 and YY11) in the KGSC in the northern HL area. **(B)** The sandstone matrix (MDAs ≤ ca. 244 Ma, Samples YY07 and YY12) in the KGSC in the northern HL area. **(C)** The sandstone matrix in the KGSC in the southern HL area. **(D)** The sandstone matrix (MDAs = 243–243 Ma) in the KGSC in the northern HL area (Ao et al., 2021). **(E)** The sandstone matrix (MDAs = 384–315 Ma) in the KGSC in the Yamansu area (Chen et al., 2019). **(F)** Sedimentary rocks in the Harlik arc. **(G)** Devonian-Permian sedimentary rocks of the Dananhu arc (Chen et al., 2019). **(H)** Late Permian–Triassic sedimentary rocks (MDAs ≤ 258 Ma) of the Dananhu arc (Chen et al., 2019). **(I)** Sedimentary rocks of the

(*Continued*)

FIGURE 12 (Continued)
Yamansu-CTS arc. Ages of $^{206}Pb/^{238}U$ and 1σ values, having concordance % >90% or <110%, which are used for density plots using DensityPlotter Version 8.5 software (Vermeesch, 2012). The age data after Supplementary Table S4.

andesitic arc field (Figure 11B), also suggesting that the sandstones were derived from a mixed source of intermediate and felsic components with a low degree of weathering, sorting and/or sedimentary rock recycling. On the plots of La/Sc vs. Ti/Zr (Figure 11C), all samples plot within the CIA field. On the La–Th–Sc diagrams, except for Sample YY11-2 (with a MDA of 271 Ma) from the northern HL area, which plots in the OIA fields, all other samples plot within the CIA field (Figure 11D).

The detrital zircon U–Pb age spectra of the sandstone matrix of the KGSC in the HL area show that the sources mainly contained Triassic, Permian-Ordovician and minor Neoproterozoic zircons, also indicating a mixed source. According to the spatiotemporal relationship of the detrital zircon age spectra, Hf isotopes and whole-rock geochemical characteristics, the sandstone samples in the N–S-trending cross-sections can be subdivided into two types of provenances:

6.2.1 Type I: Provenances of the northern Haluo area

The provenances of the sandstone matrix samples from the northern HL area changed after ca. 244 Ma. Sandstone matrix Samples YY09 and YY11 with MDAs of 316 Ma to 271 Ma were deposited in an OIA setting. They have similar spectra of zircon ages with a single age peak pattern and most analyzed grains show high positive $\varepsilon_{Hf}(t)$ values (only ca. 4% and ca. 8% analyzed grains have negative $\varepsilon_{Hf}(t)$ values), indicating that they were sourced from intraoceanic arcs. Their age and Hf isotope patterns are similar to those of the Devonian to Permian sedimentary rocks of the Dananhu arc (Figures 12G, 13A) (Chen et al., 2020) but are different from those of the Triassic sedimentary rocks of the Dananhu arc and the southern part of the HL area (Figures 12H, 13A,C) and the sedimentary rocks in the KGSC in the Yamansu area (Figures 12E, 13D), Harlik arc (Figure 12F) and Yamansu-CTS arc (Figure 12I). All of these facts indicate that these sandstone matrices (MDAs > ca. 244 Ma) were most likely sourced from the Dananhu arc.

However, the geochemical, detrital zircon age and isotope data of the sandstone matrix samples whose MDAs are younger than 244 Ma are proven to be from a continental arc. First, their geochemical signatures suggest that they were deposited in a CIA setting. Second, the zircon age spectrum of Sample YY07 has multiple peaks and a percentage of Precambrian zircon grains. They have positive to negative zircon $\varepsilon_{Hf}(t)$ values (−18.0 to +15.6) and have ca. 28% analyzed grains have negative $\varepsilon_{Hf}(t)$ values. Although Sample YY12 has a single age peak pattern

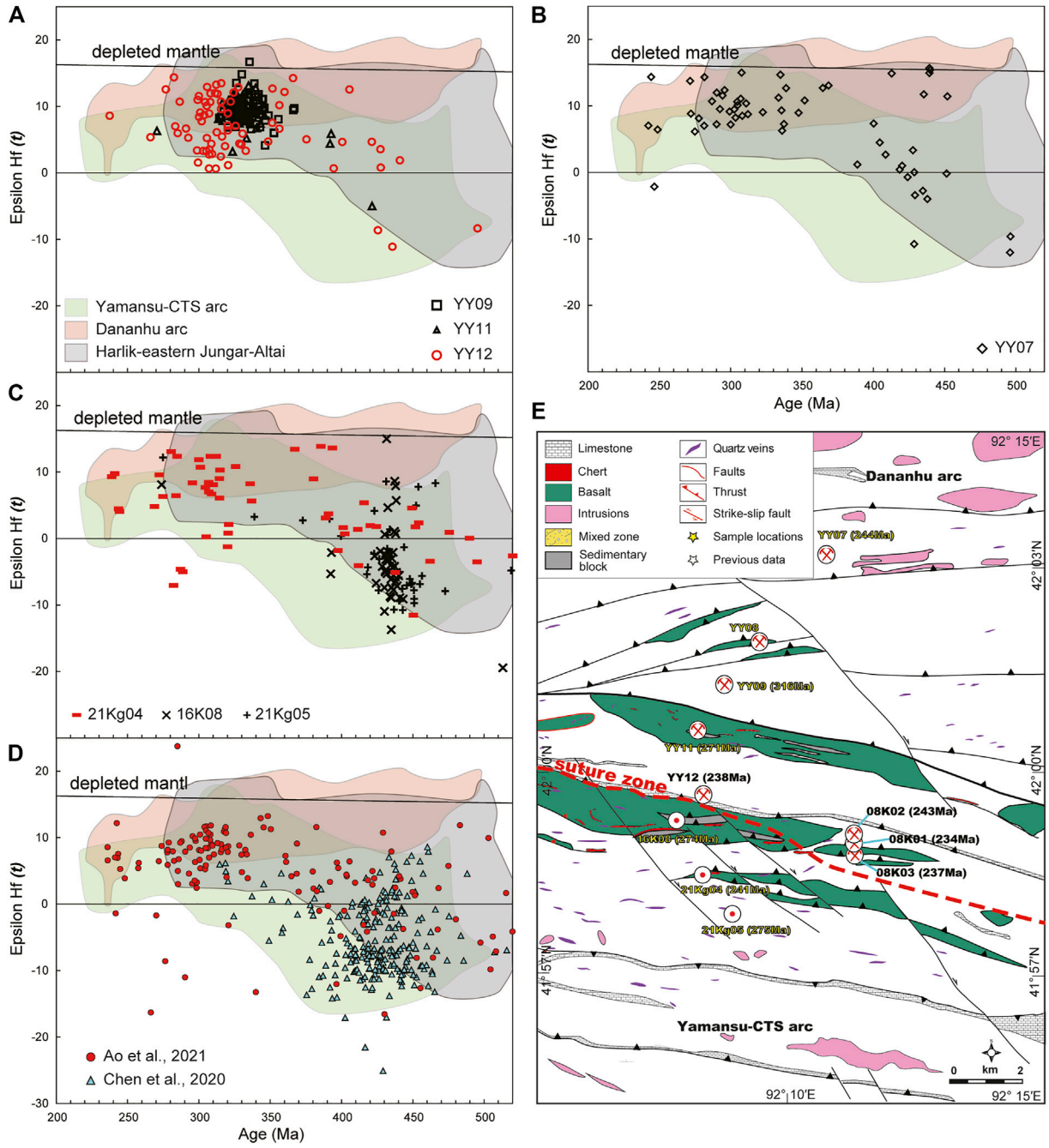

FIGURE 13
Hf isotope diagram of dated sandstones from the KGSC. **(A)** Shows that the sandstone matrix (Samples YY09 and 11) was probably derived from the Dananhu intraoceanic arc to the north. **(B)** Shows that the sandstone matrix (Samples YY07 and 12) was probably derived from the southern South Mongolian-Dananhu Andean arc to the north in the Triassic. **(C)** Shows that the sandstone matrix (Samples 16K08, 21Kg04 and 05) was probably derived from the Yamansu-CTS arc. **(D)** The Hf isotopes of the sandstone matrix samples from the KGSC in the Yamansu area (Chen et al., 2019) and the HL area (Ao et al., 2021). **(E)** Suture line between Samples YY12 and 16K08 in the N–S-trending cross-section in the HL area. The Hf isotopic data are provided in Supplementary Table S5.

similar to Samples YY07 and YY11 (Figure 12A), it displays positive to negative zircon $\varepsilon_{Hf}(t)$ values (−11.2 to +14.3) with few grains with negative zircon $\varepsilon_{Hf}(t)$ values (ca. 8%). The sample has percentages of Precambrian zircon grains but no 25Ga zircon grains, which is distinct from the detrital patterns of the Yamansu-CTS arc (Figure 12I). It also has different zircon Hf

isotope patterns to the late Paleozoic magmatic rocks of Yamansu-CTS arc (Figure 13B) and sedimentary rocks of the KGSC in south HL area (Figure 13C). In contrast, its detrital zircon age and isotopic characteristics are similar to those of Triassic sedimentary rocks in the Dananhu arc (Figure 12H) (Chen et al., 2020), the sedimentary rocks of the Harlik arc (Figure 12F) and the magmatic rocks of the South Mongolian collage (Altai, eastern Jungar and Harlik) (Figure 13B), suggesting that a small number of zircons may have been sourced from the South Mongolian collage Andean arc. These study data are consistent with our previous age and isotopic results of the sandstone matrix (with MDAs of 243 to 234 Ma) of the northern KGSC in the HL area (Figures 12D, 13D) (Ao et al., 2021).

In summary, the provenances of the sandstone matrix in the northern HL area of the KGSC were deposited and emplaced in the forearc of the Dananhu arc, and their depositional settings varied from an intraoceanic island arc to a continental Andean arc after ca. 244 Ma.

6.2.2 Type II: Continental arc provenance of the southern area

Samples 16K08, 21Kg04 and 21Kg05 were collected from the southern part of the HL area. Their MDAs are 274, 241, and 275 Ma, respectively. They have similar multiple age peak patterns with volumes of Precambrian ages similar to those of the Yamansu-CTS arc (Figures 12E,J). The high percent of analyzed grains have negative $\varepsilon_{Hf}(t)$ values (ca. 68%, 33% and 66%, respectively) are similar to those of magmatic rocks in the Yamansu-CTS arc (Figure 13C) and the KGSC in the Yamansu area (Figure 13D), suggesting that they were mainly sourced from the Yamansu-CTS continental arc.

Based on these characteristics, we can conclude that the first type of provenance for the sedimentary matrix of the KGSC in the northern HL area was mainly sourced from the Dananhu intraoceanic arc to the Andean arc after ca. 244 Ma. These results are consistent with the interpretation that the Triassic sedimentary rocks (<258 Ma) in the Dananhu arc were partly sourced from the southern South Mongolian Andean arc (Altai, eastern Junggar and Harlik) (Chen et al., 2020). However, the other type of sandstone matrix of the KGSC in the southern HL area was mainly sourced from the Yamansu-central Tianshan arc, which was similar to the KGSC in the Yamansu area (Chen et al., 2019). In summary, our study suggests that the KGSC in the HL area had a mixed provenance between the Dananhu and Yamansu-CTS arcs.

6.3 Suture zone and closure time of the Kanguer subduction complex in the Haluo area

The nature and composition of the KGSC have been widely discussed and remains controversial (Ma et al., 1997; Li, 2004; Li et al., 2008; Muhetaer et al., 2010; Chen et al., 2019; Ao et al., 2021). To date, three competing models have been proposed by previous studies and have been interpreted an the accretionary complex of the Dananhu (Li, 2004; Xiao et al., 2004; Li et al., 2005; Li et al., 2008; Ao et al., 2021), the Yamansu arc (Ma et al., 1997; Chen et al., 2019) and a mixture of the Dananhu and Yamansu arcs (Muhetaer et al., 2010; Mao Q. et al., 2021; Mao et al., 2022b).

As discussed above, our geochemical, geocryological and isotopic studies reveal that the KGSC in the HL area represents mixing of the forearc subduction mélanges which consist of the N-MORB, E-MORB and SZZ type ophiolite fragments (including gabbro, basalt, and chert) and sedimentary matrix and limestones between the Dananhu and Yamansu-CTS arcs formed by double subduction. Our study reveals that the matrices (Samples YY07, 09, 11 and 12) in the northern HL area are mainly proven to be from the Dananhu arc. However, the matrices in the southern HL area, which are represented by Samples 16K08, 21Kg 04 and 05, were mainly proven to be from the Yamansu-CTS arc. All of these data indicate that the suture line of the KGSC in the HL area is located between Samples YY12 and 16K08 in the N–S-trending section. Combined with the previous data from Ao et al. (2021), which suggest that the sedimentary matrix rocks in the middle HL area were sourced from the Triassic Dananhu Andean arc (Figure 13D), we suggest that the final suture line was located in the middle part of the HL area, as shown in Figure 10E.

As discussed above, the petrological and geochemical characteristics of the sandstone matrix together reveal that they were deposited on a convergence margin; therefore, the MDA of the detrital zircons can represent the time of deposition of these sedimentary matrix rocks (Cawood et al., 2012). In this study, the youngest sandstone matrix has a MDA of 238 Ma, and Ao et al. (2021) reported that the sandstone matrix of the KGSC in the HL area has MDAs of 243–234 Ma, suggesting that the northern Tianshan Ocean closed later than ca. 234 Ma. In addition, the mid-Late Triassic peak metamorphic ages of the eclogites in the western Tianshan (Zhang et al., 2007; Sang et al., 2017; Sang et al., 2020) and the 243–234 Ma thickened lower crust-derived adakites in the Dananhu arc (Mao Q. et al., 2021) also suggest that subduction continued in the mid-Late Triassic. Thus, we conclude that the Paleo-Asian Ocean closed later than ca. 234 Ma.

6.4 Tectonic implications

Our new detrital zircon U–Pb ages and zircon $\varepsilon_{Hf}(t)$ values of the matrix sandstone reveal that the KGSC experienced double-directional subduction and that the suture line is located in the middle of the KGSC in the HL area. The northern samples of the Kanguer subduction in the HL area were deposited in an oceanic-island-arc setting before ca. 244 Ma and changed to an Andean-type arc setting after ca. 244 Ma. Furthermore, the southern samples were deposited in a continental-island-arc setting

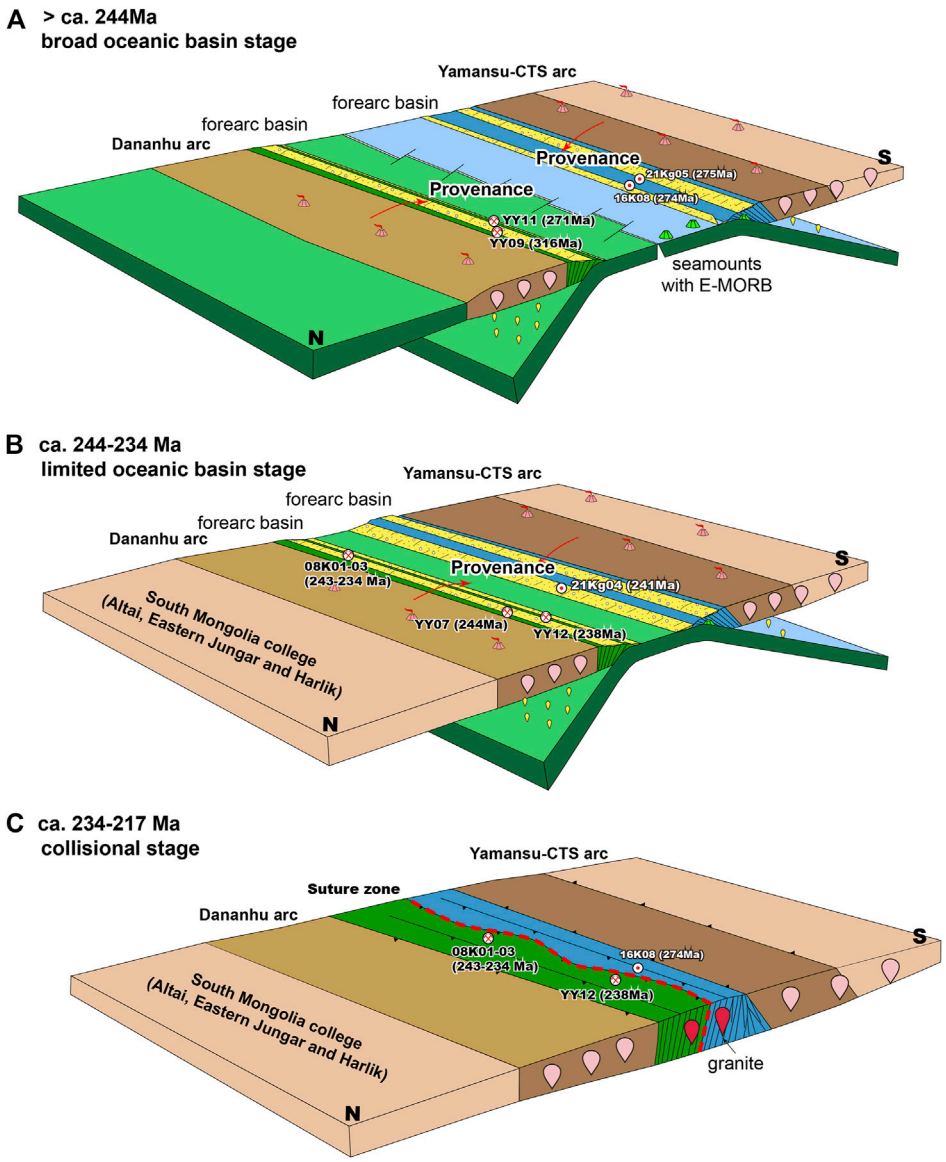

FIGURE 14
Tectonic model showing two stages of evolution in the eastern Tianshan. **(A)** Before the Middle Triassic (>ca. 244 Ma), the northern Tianshan Ocean, a branch of the Paleo-Asian Ocean, remained open preventing material exchanges on both sides and was doubly subducting. Blocks of N-MORB, SSZ-affinity oceanic crust, limestone, and chert were accreted to the forearc of the Dananhu arc and N-MORB, E-MORB-affinity oceanic crust, limestone, and chert accreted to the forearc of Yamansu-CTS arcs of the growing Kanguer accretionary complex. **(B)** In the Middle to Late Triassic (244–234 Ma), the northern Tianshan Ocean remained open and was subducted on both sides, and the sandstone matrices on both sides of the accretionary complexes have MDAs of 244 to 234 Ma. The convergence between the Dananhu Arc and South Mongolian collage (Altai, eastern Jungar and Harlik Arc) led to Precambrian zircon input in the sandstone matrix of the AC of the Dananhu Arc. **(C)** In the Late Triassic (234–217 Ma), the northern Tianshan Ocean closed by double subduction, and the Dananhu Andean arc was amalgamated with the Yamansu-CTS continental arc. Large syncollisional granodiorite plutons intruded the two arcs and their accretionary complexes.

(Figures 11A,B). Therefore, we updated our tectonic model of the eastern Tianshan in the southern Altaids (Figure 14).

The northern Tianshan ocean basin was a broad ocean prevented material exchanges between the Dananhu and Yamansu arcs before ca. 244 Ma (Figure 14A), the sandstone matrices in the northern HL area have simple detrital U–Pb ages and zircon Hf isotope patterns (Figures 6, 12B, 13A). This interpretation is consistent with the detrital zircon age and isotopic studies of the sedimentary rocks of the Dananhu and Yamansu-CTS arcs (Chen et al., 2020) and the sandstone matrix in the KGSC in the Yamansu area (Chen et al., 2019). From ca. 244 Ma to 234 Ma (Figure 14B), the northern Tianshan Ocean was

a limited oceanic basin and was still subducting on both sides. The Dananhu arc converged with the South Mongolian collage (Altai, eastern Jungar and Harlik arc systems) and formed an Andean continental arc. The Precambrian zircons of the South Mongolian collage were deposited into the sedimentary matrix of the accretionary complex of the Dananhu arc (Chen et al., 2019; Ao et al., 2021), such as Sample YY07. These tectonic processes also induced the Dananhu arc crust to thicken and to form volumes of 243–234 Ma thickened lower crust-derived adakites in the Dananhu arc (Mao Q. et al., 2021). Combined with large-scale syncollisional granites intruded in the eastern Tianshan in the Late Triassic (232–217 Ma) (Li et al., 2012; Wang et al., 2016; Wu et al., 2016; Mao et al., 2022a) and the rapid and strong regional uplift and denudation of the Tianshan orogen in the Late Triassic (Gong et al., 2021), we suggest that the closure time of the northern Tianshan Ocean was most likely during the Late Triassic (Ao et al., 2021; Mao et al., 2022a) (Figure 14C). The KGSC was thrust southward during the final amalgamated processes.

7 Conclusion

(1) The KGSC in the HL area was thrusted top-to-the-south and is characterized by a block-in-matrix structure among the different oceanic fragments and sedimentary rocks. The basaltic blocks of the northern HL area yielded a zircon U–Pb age of 257 Ma and have N-MORB geochemical signatures.
(2) The geochemistry and composition of the sandstone matrix of the northern Kanguer subduction complex in the HL area suggest that the Dananhu arc has varied from an OIA to a CIA setting since ca. 244 Ma. However, the sandstone matrix of the southern Kanguer subduction complex in the HL area was always deposited in a CIA setting during the late Paleozoic.
(3) The northern Tianshan Ocean experienced double subduction, and the suture line is located between Samples YY12 and 16K08 in the middle of the HL area. The MDAs of the KGSC matrix sandstones in the HL area have an age range of 316 Ma to 238 Ma, which indicates that the northern Tianshan Ocean was still open at 238 Ma, and the final collision occurred during 234–217 Ma.

Data availability statement

The original contributions presented in the study are included in the article/Supplementary Material, further inquiries can be directed to the corresponding authors.

Author contributions

QM and WX initiated the idea and designed the studies. QM, MS, and SA finished the field, petrology, and geochemical experiments. DS and RL performed the zircon dating and Hf isotopic analysis. HW and ZT processed the geochemical data. QM and MS write the original manuscript. WX works with the geological model and finalized the manuscript. All authors have been involved in the study.

Funding

This study was financially supported by the National Natural Science Foundation of China (41888101, 41822204), One Hundred Talent Program of the Chinese Academy of Sciences (E2250403), Science and Technology Major Project of Xinjiang Uygur Autonomous Region, China (2021A03001&4), the Chinese Ministry of Land and Resources for the Public Welfare Industry Research (201411026-1), the "Light of West China" Program of the CAS (2017-XBQNXZ-B-013, 2018-XBYJRC-003), and the Project of China-Pakistan Joint Research Center on Earth Sciences of the CAS (131551KYSB20200021). This is a contribution to IGCP 662 and IGCP 710.

Conflict of interest

Author QM was employed by the company Redrock Mining Co. Ltd.

The remaining authors declare that the research was conducted in the absence of any commercial or financial relationships that could be construed as a potential conflict of interest.

Publisher's note

Supplementary material

The Supplementary Material for this article can be found online at: https://www.frontiersin.org/articles/10.3389/feart.2022.1089700/full#supplementary-material

SUPPLEMENTARY TABLE S1
U–Pb ages of detrital zircons of sedimentary rocks from the KGSC in the Haluo area. HigHLy discordant analyses (concord% <90% or >110%) are considered unusable, displayed in strikethrough text, and were not included in the concordia diagrams. Concord% = 100*(^{207}Pb/^{206}Pb) age/(^{206}Pb/^{238}U) age for age >1,500 Ma, or 100*(^{207}Pb/^{235}U) age/(^{206}Pb/^{238}U) age for age <1,500 Ma.

SUPPLEMENTARY TABLE S2
Lu–Hf isotope data of zircons from the sedimentary matrix rocks in the KGSC in the Haluo area.

SUPPLEMENTARY TABLE S3
Whole-rock major and trace element data of basalts and sandstone matrix from the KGSC in the Haluo area.

SUPPLEMENTARY TABLE S4
Zircon U–Pb ages of the sedimentary rocks around the KGSC in the eastern Tianshan.

SUPPLEMENTARY TABLE S5
Zircon Hf isotope data of the magmatic rocks of the Dananhu arc, Yanmansu-CTS arc and South Mongolian collage (Altai, eastern Junggar and Harlik arcs).

References

Ao, S. J., Mao, Q. G., Windley, B. F., Song, D. F., Zhang, Z. Y., Zhang, J. E., et al. (2021). The youngest matrix of 234Ma of the kanguer accretionary mélange containing blocks of N-MORB basalts: Constraints on the northward subduction of the paleo-asian kanguer Ocean in the eastern tianshan of the southern Altaids. *Int. J. Earth Sci.* 110, 791–808. doi:10.1007/s00531-021-01990-5

Ao, S. J., Xiao, W. J., Windley, B. F., Mao, Q. G., Zhang, J. E., and Zhang, Z. Y. (2020). Ordovician to Early Permian accretionary tectonics of Eastern Tianshan: Insights from Kawabulak ophiolitic melange, granitoid, and granitic gneiss. *Geol. J.* 55 (1), 280–298. doi:10.1002/gj.3371

Bazhenov, M. L., Collins, A. Q., Degtyarev, K. E., Levashova, N. M., Mikolaichuk, A. V., Pavlov, V. E., et al. (2003). Paleozoic northward drift of the north tien Shan (central Asia) as revealed by ordovician and carboniferous paleomagnetism. *Tectonophysics* 366 (1), 113–141. doi:10.1016/s0040-1951(03)00075-1

Bhatia, M., and Crook, K. W. (1986). Trace element characteristics of graywackes and tectonic setting discrimination of sedimentary basins. *Contr. Mineral. Pet.* 92, 181–193. doi:10.1007/bf00375292

Boynton, W. V. (1984). "Geochemistry of the rare Earth elements: Meteorite study," in *Rare Earth element geochemistry*. Editor P. Henderson (Amsterdam: Elsevier), 63–114.

Buchan, C., Pfänder, J., Kröner, A., Brewer, T. S., Tomurtogoo, O., Tomurhuu, D., et al. (2002). Timing of accretion and collisional deformation in the central asian orogenic belt: Implications of granite geochronology in the bayankhongor ophiolite zone. *Chem. Geol.* 192, 23–45. doi:10.1016/s0009-2541(02)00138-9

Cawood, P. A., Hawkesworth, C. J., and Dhuime, B. (2012). Detrital zircon record and tectonic setting. *Geology* 40 (10), 875–878. doi:10.1130/g32945.1

Chen, Z., Xiao, W., Windley, B. F., Schulmann, K., Mao, Q., Zhang, Z., et al. (2019). Composition, provenance, and tectonic setting of the southern kangurtag accretionary complex in the eastern tianshan, NW China: Implications for the late paleozoic evolution of the north Tianshan ocean. *Tectonics* 38 (8), 2779–2802. doi:10.1029/2018tc005385

Chen, Z., Xiao, W., Windley, B. F., Schulmann, K., Mao, Q., Zhang, Z., et al. (2020). Latest permian–early triassic arc amalgamation of the eastern tianshan (NW China): Constraints from detrital zircons and Hf isotopes of devonian–triassic sediments. *Geol. J.* 55, 1708–1727. doi:10.1002/gj.3540

Coleman, R. G. (1989). Continental growth of northwest China. *Tectonics* 8, 621–635. doi:10.1029/tc008i003p00621

Coutts, D. S., Matthews, W. A., and Hubbard, S. M. (2019). Assessment of widely used methods to derive depositional ages from detrital zircon populations. *Geosci. Front.* 10 (4), 1421–1435. doi:10.1016/j.gsf.2018.11.002

Dobretsov, N. L., Berzin, N. A., and Buslov, M. M. (1995). Opening and tectonic evolution of the paleo-Asian ocean. *Int. Geol. Rev.* 35, 335–360. doi:10.1080/00206819509465407

Du, L., Long, X., Yuan, C., Zhang, Y., Huang, Z., Sun, M., et al. (2018a). Petrogenesis of Late Paleozoic diorites and A-type granites in the central Eastern Tianshan, NW China: Response to post-collisional extension triggered by slab breakoff. *Lithos* 318-319, 47–59. doi:10.1016/j.lithos.2018.08.006

Du, L., Long, X., Yuan, C., Zhang, Y., Huang, Z., Wang, X., et al. (2018b). Mantle contribution and tectonic transition in the aqishan-yamansu belt, eastern tianshan, NW China: Insights from geochronology and geochemistry of early carboniferous to early permian felsic intrusions. *Lithos* 304-307, 230–244. doi:10.1016/j.lithos.2018.02.010

Du, L., Zhang, Y., Huang, Z., Li, X.-P., Yuan, C., Wu, B., et al. (2019). Devonian to carboniferous tectonic evolution of the Kangguer Ocean in the Eastern Tianshan, NW China: Insights from three episodes of granitoids. *Lithos* 350-351, 105243. doi:10.1016/j.lithos.2019.105243

Du, L., Zhu, H., Yuan, C., Zhang, Y., Huang, Z., Li, X.-P., et al. (2021). Paleozoic crustal evolution and tectonic switching in the northeastern tianshan: Insights from zircon Hf isotopes of granitoids. *J. Geol. Soc. Lond.* 178 (2), jgs2020–035. doi:10.1144/jgs2020-035

Du, L., Zhu, H., Yuan, C., Zhang, Y., Long, X., Li, X. P., et al. (2020). Paleozoic crustal evolution and tectonic switching in the northeastern tianshan: Insights from zircon Hf isotopes of granitoids. *J. Geol. Soc. Lond.* 178, jgs2020–035. doi:10.1144/jgs2020-035

Festa, A., Pini, G. A., Ogata, K., and Dilek, Y. (2019). Diagnostic features and field-criteria in recognition of tectonic, sedimentary and diapiric mélanges in orogenic belts and exhumed subduction-accretion complexes. *Gondwana Res.* 74, 7–30. doi:10.1016/j.gr.2019.01.003

Floyd, P. A., and Leveridge, B. E. (1987)., 144. London, 531–542. doi:10.1144/gsjgs.144.4.0531Tectonic environment of the devonian gramscatho basin, south cornwall: Framework mode and geochemical evidence from turbiditic sandstones*J. Geol. Soc. Lond.*

Floyd, P. A., Shail, R., Leveridge, B., and Franke, W. (1991). Geochemistry and provenance of Rhenohercynian synorogenic sandstones: Implications for tectonic environment discrimination. *Geol. Soc. Lond. Spec. Publ.* 57, 173–188. doi:10.1144/gsl.sp.1991.057.01.14

Gao, J., and Klemd, R. (2003). Formation of HP-lt rocks and their tectonic implications in the Western tianshan orogen, NW China: Geochemical and age constraints. *Lithos* 66 (1-2), 1–22. doi:10.1016/s0024-4937(02)00153-6

Gong, L., Kohn, B. P., Zhang, Z., Xiao, B., Wu, L., and Chen, H. (2021). Exhumation and preservation of Paleozoic porphyry Cu deposits: Insights from the Yandong deposit, southern Central Asian orogenic belt. *Econ. Geol.* 116 (3), 607–628. doi:10.5382/econgeo.4812

Han, J., Chen, H., Jiang, H., Zhao, L., Zhang, W., and Lai, C. K. (2019). Genesis of the paleozoic aqishan-yamansu arc-basin system and Fe (-Cu) mineralization in the eastern tianshan, NW China. *Ore Geol. Rev.* 105, 55–70. doi:10.1016/j.oregeorev.2018.12.012

Han, Y., and Zhao, G. (2018). Final amalgamation of the tianshan and junggar orogenic collage in the southwestern central asian orogenic belt: Constraints on the closure of the paleo-Asian ocean. *Earth-Science Rev.* 186, 129–152. doi:10.1016/j.earscirev.2017.09.012

Hou, T., Zhang, Z., Santosh, M., Encarnacion, J., Zhu, J., and Luo, W. (2014). Geochronology and geochemistry of submarine volcanic rocks in the Yamansu iron deposit, Eastern Tianshan Mountains, NW China: Constraints on the metallogenesis. *Ore Geol. Rev.* 56, 487–502. doi:10.1016/j.oregeorev.2013.03.008

Hawkins, J. W. (2003). Geology of supra-subduction zones-Implications for the origin of ophiolites. *Geol. Soc. Am. Spec. Pap.* 373, 227–268. doi:10.1130/0-8137-2373-6.227

Hsü, K. (1968). Principles of mélanges and their bearing on the Franciscan-Knoxville Paradox. *Geol. Soc. Am. Bull.* 78, 1063–1174. doi:10.1130/0016-7606(1968)79[1063:pomatb]2.0.co;2

Hu, A., Jahn, B. M., Zhang, G., Chen, Y., and Zhang, Q. (2000). Crustal evolution and phanerozoic crustal growth in northern Xinjiang: Nd isotopic evidence, Part I. Isotopic characterization of basement rocks. *Tectonophysics* 328, 15–51. doi:10.1016/s0040-1951(00)00176-1

Isozaki, Y., Maruyama, S., and Furuoka, F. (1990). Accreted oceanic materials in Japan. *Tectonophysics* 181 (1-4), 179–205. doi:10.1016/0040-1951(90)90016-2

Kusky, T. M., Windley, B. F., Safonova, I., Wakita, K., Wakabayashi, J., Polat, A., et al. (2013). Recognition of ocean plate stratigraphy in accretionary orogens through Earth history: A record of 3.8 billion years of sea floor spreading, subduction, and accretion. *Gondwana Res.* 24 (2), 501–547. doi:10.1016/j.gr.2013.01.004

Kusky, T., Wang, J., Wang, L., Huang, B., Ning, W., Fu, D., et al. (2020). Mélanges through time: Life cycle of the world's largest Archean mélange compared with Mesozoic and Paleozoic subduction-accretion-collision mélanges. *Earth-Science Rev.* 209, 103303. doi:10.1016/j.earscirev.2020.103303

Li, D.-F., Zhang, L., Chen, H.-Y., Hollings, P., Cao, M.-J., Fang, J., et al. (2016). Geochronology and geochemistry of the high Mg dioritic dikes in Eastern Tianshan, NW China: Geochemical features, petrogenesis and tectonic implications. *J. Asian Earth Sci.* 115, 442–454. doi:10.1016/j.jseaes.2015.10.018

Li, J. Y., He, G. Q., Xu, X., Li, H. Q., Sun, G. H., Yang, T. N., et al. (2006). Crustal tectonic framework of northern Xinjiang and adjacent and its formation. *Acta Geol. Sin.* 80, 149–168. (in Chinese with English abstract).

Li, J. Y. (2004). Late neoproterozoic and paleozoic tectonic framework and evolution of eastern Xinjiang, NW China. *Geol. Rev.* 50, 304–322.

Li, Q. G., Liu, S. W., Song, B., Wang, Y. B., and Chen, Y. (2009). Late mesoproterozoic to paleozoic tectonothermal events in the eastern segment of the central tianshan tectonic zone of northwestern China: Constraints from SHRIMP zircon geochronology. *Earth Sci. Front.* 16, 175–184. doi:10.1016/S1874-8651(10)60080-4

Li, S., Wang, T., Wilde, S. A., Tong, Y., Hong, D., and Guo, Q. (2012). Geochronology, petrogenesis and tectonic implications of Triassic granitoids from Beishan, NW China. *Lithos* 134-135, 123–145. doi:10.1016/j.lithos.2011.12.005

Li, W. Q., Ma, H., Wang, R., and Xia, B. (2008). SHRIMP dating and Nd-Sr isotopic Tracing of Kangguertage ophiolite in eastern Tianshan, Xinjiang. *Acta Petrol. Sin.* 24 (4), 773–780. (in Chinese with English abstract).

Li, W. Q., Xia, B., Wu, G. G., Wang, H., and Wang, R. (2005). Kangguertage ophiolite and tectonic significance, Shanshan, Xinjiang China. *Acta Petrol. Sin.* 21, 1617–1632. (in Chinese with English abstract).

Liu, S., Guo, Z., Zhang, Z., Qiugen, L. I., and Zheng, H. (2004). Nature of the Precambrian metamorphic blocks in the eastern segment of Central Tianshan: Constraint from geochronology and Nd isotopic geochemistry. *Sci. China Ser. D-Earth. Sci.* 47 (12), 1085–1094. doi:10.1360/03yd0177

Long, X., Wu, B., Sun, M., Yuan, C., Xiao, W., and Zuo, R. (2020). Geochronology and geochemistry of Late Carboniferous dykes in the Aqishan–Yamansu belt, eastern Tianshan: Evidence for a post-collisional slab breakoff. *Geosci. Front.* 11 (1), 347–362. doi:10.1016/j.gsf.2019.06.003

Lu, W. J., Chen, H. Y., Zhang, L., Han, J. S., Xiao, B., Li, D. F., et al. (2017). Age and geochemistry of the intrusive rocks from the Shaquanzi-Hongyuan Pb–Zn mineral district: Implications for the Late Carboniferous tectonic setting and Pb–Zn mineralization in the Eastern Tianshan, NW China. *Lithos* 294-295, 97–111. doi:10.1016/j.lithos.2017.10.009

Luo, T., Liao, Q.-A., Zhang, X.-H., Chen, J.-P., Wang, G.-C., and Huang, X. (2016). Geochronology and geochemistry of carboniferous metabasalts in eastern tianshan, central Asia: Evidence of a back-arc basin. *Int. Geol. Rev.* 58 (6), 756–772. doi:10.1080/00206814.2015.1114433

Ma, R. S., Shu, L. S., and Sun, J. (1997). *Tectonic evolution and metalogeny of eastern tianshan mountains*. Beijing: Geological Publishing House.

Ma, X., Shu, L., Meert, J. G., and Li, J. (2014). The paleozoic evolution of central tianshan: Geochemical and geochronological evidence. *Gondwana Res.* 25 (2), 797–819. doi:10.1016/j.gr.2013.05.015

Mader, D., and Neubauer, F. (2004). Provenance of palaeozoic sandstones from the carnic alps (Austria): Petrographic and geochemical indicators. *Int. J. Earth Sci.* 93 (2), 262–281. doi:10.1007/s00531-004-0391-x

Mao, Q., Ao, S., Windley, B. F., Wang, J., Li, Y., and Xiao, W. (2021a). Middle Triassic lower crust-derived adakitic magmatism: Thickening of the Dananhu intra-oceanic arc and its implications for arc–arc amalgamation in the Eastern Tianshan (NW China). *Geol. J.* 56 (6), 3137–3154. doi:10.1002/gj.4095

Mao, Q., Ao, S., Windley, B. F., Zhang, Z., Sang, M., Tan, Z., et al. (2022a). Middle-late triassic southward-younging granitoids: Tectonic transition from subduction to collision in the eastern tianshan-beishan orogen, NW China. *GSA Bull.* 134, 2206–2224. doi:10.1130/b36172.1

Mao, Q. G., Wang, J. B., Xiao, W. J., Fang, T. H., Wang, N., and Yu, M. J. (2014a). The deiscovery of low-Carboniferous arc volcanic rocks and its tectonic signifance at the Kalatage area in the central Tianshan, eastern Tianshan Mountans, Xinjiang, NW China. *Acta Geol. Sin.* 88, 1790–1799. (in Chinese with English abstract).

Mao, Q. G., Wang, J. B., Xiao, W. J., Windley, B. F., Schulmann, K., Ao, S. J., et al. (2021b). From ordovician nascent to early permian mature arc in the southern Altaids: Insights from the kalatage inlier in the eastern tianshan, NW China. *Geosphere* 17, 647–683. doi:10.1130/ges02232.1

Mao, Q. G., Wang, J. B., Xiao, W. J., Windley, B. F., Schulmann, K., Yu, M. J., et al. (2019). Mineralization of an intra-oceanic arc in an accretionary orogen: Insights from the Early Silurian Honghai volcanogenic massive sulfide Cu-Zn deposit and associated adakites of the Eastern Tianshan (NW China). *GSA Bull.* 131, 803–830. doi:10.1130/b31986.1

Mao, Q. G., Xiao, W. J., Fang, T. H., Windley, B. F., Sun, M., Ao, S. J., et al. (2014b). Geochronology, geochemistry and petrogenesis of early permian alkaline magmatism in the eastern tianshan: Implications for tectonics of the southern Altaids. *Lithos* 190-191, 37–51. doi:10.1016/j.lithos.2013.11.011

Mao, Q., Xiao, W., Huang, P., Ao, S., Song, D. F., Zhang, J. E., et al. (2022b). Deformational history of the kanguer subduction complex in the eastern tianshan (NW China): Implications for paleozoic-triassic multiple accretionary tectonics of the southern Altaids. *Tectonics* 41, e2022TC007527. In press. doi:10.1029/2022tc007527

Maynard, J., Valloni, R., and Yu, H.-S. (1982). Composition of modern deep-sea sands from arc-related basins. *Geol. Soc. Lond. Spec. Publ.* 10, 551–561. doi:10.1144/gsl.sp.1982.010.01.36

McLennan, S. M., Hemming, S., McDaniel, D. K., Hanson, G. N., Johnsson, M. J., and Basu, A. (1993). "Geochemical approaches to sedimentation, provenance, and tectonics," in *Processes controlling the composition of clastic sediments* (United States: Geological Society of America), 0.

Muhetaer, Z., Wu, Z., and Parati, A. (2010). Relationship between tectonic evolution and polymetallic mineralization of the east tianshan plate suture zone. *Earth Sci.* 30 (2), 245–253. (in Chinese with English abstract).

Myashiro, A. (1974). Volcanic series in island arc and active continental margins. *Am. J. Sci.* 274, 321–355. doi:10.2475/ajs.274.4.321

Pearce, J. A. (2008). Geochemical fingerprinting of oceanic basalts with applications to ophiolite classification and the search for Archean oceanic crust. *Lithos* 100, 14–48. doi:10.1016/j.lithos.2007.06.016

Pettijohn, F. J., Potter, P. E., and Siever, R. (1972). *Sand and sandstone*. New York: Springer-Verlag.

Potter, P. E. (1978). Petrology and chemistry of modern big river sands. *J. Geol.* 86, 423–449. doi:10.1086/649711

Qin, K. Z., Su, B. X., Sakyi, P. A., Tang, D. M., Li, X. H., Sun, H., et al. (2011). SIMS zircon U-Pb geochronology and Sr-Nd isotopes of Ni-Cu-Bearing Mafic-Ultramafic Intrusions in Eastern Tianshan and Beishan in correlation with flood basalts in Tarim Basin (NW China): Constraints on a ca. 280 Ma mantle plume. *Am. J. Sci.* 311, 237–260. doi:10.2475/03.2011.03

Raymond, L. A. (2019). Perspectives on the roles of melanges in subduction accretionary complexes: A review. *Gondwana Res.* 74, 68–89. doi:10.1016/j.gr.2019.03.005

Sang, M., Xiao, W., Bakirov, A., Orozbaev, R., Sakiev, K., and Zhou, K. (2017). Oblique wedge extrusion of UHP/HP complexes in the late triassic: Structural analysis and zircon ages of the atbashi complex, south tianshan, Kyrgyzstan. *Int. Geol. Rev.* 59, 1369–1389. doi:10.1080/00206814.2016.1241163

Sang, M., Xiao, W., and Windley, B. F. (2020). Unravelling a Devonian–Triassic seamount chain in the South Tianshan high-pressure/ultrahigh-pressure accretionary complex in the Atbashi area (Kyrgyzstan). *Geol. J.* 55 (3), 2300–2317. doi:10.1002/gj.3776

Şengör, A. M. C., Natal'in, B. A., and Burtman, U. S. (1993). Evolution of the Altaid tectonic collage and Paleozoic crustal growth in Eurasia. *Nature* 364, 209–304. doi:10.1038/364299a0

Şengör, A. M. C., and Natal'in, B. (1996). Turkic-type orogeny and its role in the making of the continental crust. *Annu. Rev. Earth Planet. Sci.* 24, 263–337. doi:10.1146/annurev.earth.24.1.263

Sun, S. S., and McDonough, W. F. (1989). "Chemical and isotopic systematic of oceanic basalts: Implicattions for mantle composition and process," in *Magmatism in the ocean basins*. Editors A. D. Sauders and M. J. Norry (London: Geological Society Special Publication), 3l3–345.

Vermeesch, P. (2012). On the visualisation of detrital age distributions. *Chem. Geol.* 312-313, 190–194. doi:10.1016/j.chemgeo.2012.04.021

Wakabayashi, J. (2015). Anatomy of a subduction complex: Architecture of the franciscan complex, California, at multiple length and time scales. *Int. Geol. Rev.* 57 (5-8), 669–746. doi:10.1080/00206814.2014.998728

Wakabayashi, J. (2019). Sedimentary compared to tectonically-deformed serpentinites and tectonic serpentinite mélanges at outcrop to petrographic scales: Unambiguous and disputed examples from California. *Gondwana Res.* 74, 51–67. doi:10.1016/j.gr.2019.04.005

Wakita, K. (2015). OPS mélange: A new term for mélanges of convergent margins of the world. *Int. Geol. Rev.* 57 (5-8), 529–539. doi:10.1080/00206814.2014.949312

Wang, G. C., Zhang, M., Feng, J. L., Liao, Q. A., Zhang, X. H., Kang, L., et al. (2019). New understanding of the tectonic framework and evolution during the Neoproterozoic-Paleozoic era in the East Tianshan mountains. *Joural Geomechanics* 25 (5), 798–819. doi:10.12090/j.issn.1006-6616.2019.25.05.066

Wang, J. B., Wang, Y. W., and He, Z. J. (2006). Ore deposits as a guide to the tectonic evolution in the East Tianshan Mountains, NW China. *Geol. China* 33, 461–469. (in Chinese with English abstract).

Wang, Y., Chen, H., Han, J., Chen, S., Huang, B., Li, C., et al. (2018). Paleozoic tectonic evolution of the Dananhu-Tousuquan island arc belt, Eastern Tianshan: Constraints from the magmatism of the Yuhai porphyry Cu deposit, Xinjiang, NW China. *J. Asian Earth Sci.* 153, 282–306. doi:10.1016/j.jseaes.2017.05.022

Wang, Y. H., Xue, C. J., Liu, J. J., and Zhang, F. F. (2016). Geological, geochronological, geochemical, and Sr-Nd-O-Hf isotopic constraints on origins

of intrusions associated with the Baishan porphyry Mo deposit in eastern Tianshan, NW China. *Min. Depos.* 51, 953–969. doi:10.1007/s00126-016-0646-z

Wilhem, C., Windley, B. F., and Stampfli, G. M. (2012). The Altaids of central Asia: A tectonic and evolutionary innovative review. *Earth-Science Rev.* 113 (3-4), 303–341. doi:10.1016/j.earscirev.2012.04.001

Wilson, M. (2001). *Igneous petrogenesis: A global tectonic approach*. Amsterdam: Kuwer Academic, 245–285.

Windley, B. F., Alexeiev, D., Xiao, W., Kröner, A., and Badarch, G. (2007)., 164. London, 31–47. doi:10.1144/0016-76492006-022Tectonic models for accretion of the central asian orogenic belt*J. Geol. Soc. Lond.*

Wood, D. A. (1980). The application of a Th-Hf-Ta diagram to problems of tectonomagmatic classification and to establishing the nature of crustal contamination of basaltic lavas of the British Tertiary volcanic province. *Earth & Planet. Sci. Lett.* 50, 11–30. doi:10.1016/0012-821x(80)90116-8

Wu, Y. S., Zhou, K. F., Li, N., and Chen, Y. J. (2016). Zircon U–Pb dating and Sr–Nd–Pb–Hf isotopes of the ore-associated porphyry at the giant Donggebi Mo deposit, Eastern Tianshan, NW China. *Ore Geol. Rev.* 2 (2), 794–807. doi:10.1016/j.oregeorev.2016.02.007

Xia, L. Q., Xu, X. Y., Xia, Z. C., Li, X. M., Ma, Z. P., and Wang, L. S. (2004). Petrogenesis of Carboniferous rift-related volcanic rocks in the Tianshan, northwestern China. *Geol. Soc. Am. Bull.* 116, 419–433. doi:10.1130/b25243.1

Xiao, W. J., Mao, Q. G., Windley, B. F., Qu, J. F., Zhang, J. E., Ao, S. J., et al. (2010). Paleozoic multiple accretionary and collisional processes of the Beishan orogenic collage. *Am. J. Sci.* 310, 1553–1594. doi:10.2475/10.2010.12

Xiao, W. J., Windley, B. F., Han, C. M., Liu, W., Wan, B., Zhang, J. E., et al. (2018). Late Paleozoic to early Triassic multiple roll-back and oroclinal bending of the Mongolia collage in Central Asia. *Earth-Science Rev.* 186, 94–128. doi:10.1016/j.earscirev.2017.09.020

Xiao, W. J., Windley, B. F., Sun, S., Li, J. L., Huang, B. C., Han, C. M., et al. (2015). A tale of amalgamation of three permo-triassic collage systems in central Asia: Oroclines, sutures, and terminal accretion. *Annu. Rev. Earth Planet. Sci.* 43 (1), 477–507. doi:10.1146/annurev-earth-060614-105254

Xiao, W. J., Zhang, L. C., Qin, K. Z., Sun, S., and Li, J. L. (2004). Paleozoic accretionary and collisional tectonics of the Eastern Tianshan (China): Implications for the continental growth of central Asia. *Am. J. Sci.* 304, 370–395. doi:10.2475/ajs.304.4.370

Yan, Z., Fu, C., Wang, Z., Yan, Q., Chen, L., and Chen, J. (2016). Late Paleozoic subduction–accretion along the southern margin of the North Qinling terrane, central China: Evidence from zircon U-Pb dating and geochemistry of the Wuguan Complex. *Gondwana Res.* 30, 97–111. doi:10.1016/j.gr.2015.05.005

Zhang, J., Xiao, W., Han, C., Ao, S., Chao, Y., Min, S., et al. (2012). Kinematics and age constraints of deformation in a Late Carboniferous accretionary complex in Western Junggar, NW China. *Gondwana Res.* 19, 958–974. doi:10.1016/j.gr.2010.10.003

Zhang, L., Ai, Y., Li, X., Rubatto, D., Song, B., Williams, S., et al. (2007). Triassic collision of Western Tianshan orogenic belt, China: Evidence from SHRIMP U–Pb dating of zircon from HP/UHP eclogitic rocks. *Lithos* 96 (1-2), 266–280. doi:10.1016/j.lithos.2006.09.012

Zhang, Y., Sun, M., Yuan, C., Long, X., Jiang, Y., Li, P., et al. (2018). Alternating trench advance and retreat: Insights from paleozoic magmatism in the eastern tianshan, central asian orogenic belt. *Tectonics* 37, 2142–2164. doi:10.1029/2018tc005051

Zhao, L., Chen, H., Hollings, P., and Han, J. (2019). Late paleozoic magmatism and metallogenesis in the aqishan-yamansu belt, eastern tianshan: Constraints from the bailingshan intrusive complex. *Gondwana Res.* 65, 68–85. doi:10.1016/j.gr.2018.08.004

Zhou, M. F., Lesher, C. M., Yang, Z. X., Li, J. W., and Sun, M. (2004). Geochemistry and petrogenesis of 270 Ma Ni-Cu-(PGE) sulfide-bearing mafic intrusions in the huangshan district, eastern Xinjiang, northwest China: Implications for the tectonic evolution of the central asian orogenic belt. *Chem. Geol.* 209, 233–257. doi:10.1016/j.chemgeo.2004.05.005